This is to certify that the

thesis entitled

THE MANUFACTURING, TESTING, AND ANALYSIS OF A DEVICE FOR THE TESTING OF A MICROSCALE HEAT EXCHANGER

presented by

DANIEL D. FICKES

has been accepted towards fulfillment
of the requirements for

MASTERS degree in **MECHANICAL ENGINEERING**

Craig W. Somerton
Major professor

Date 12/9/02

[redacted]

PLACE IN RETURN BOX to remove this checkout from your record.
TO AVOID FINES return on or before date due.
MAY BE RECALLED with earlier due date if requested.

DATE DUE	DATE DUE	DATE DUE

THE MANUFACTURING, TESTING, AND ANALYSIS OF A DEVICE FOR THE TESTING OF A MICROSCALE HEAT EXCHANGER

By

Daniel D. Fickes

A THESIS

Submitted to
Michigan State University
in partial fulfillment of the requirements
for the degree of

MASTER OF SCIENCE

Department of Mechanical Engineering

2002

ABSTRACT

THE MANUFACTURING, TESTING, AND ANALYSIS OF A DEVICE FOR THE TESTING OF A MICROSCALE HEAT EXCHANGER

By

Daniel D. Fickes

In this work, a testing apparatus was manufactured, tested, and analyzed for a microscale heat exchanger. The device simulated the heat transfer from a computer chip by means of a single phase microscale heat exchanger. Water was used as the cooling fluid for a range of volume flow rates. The motivation of this thesis was to develop the concept of liquid cooled microprocessor chips. Faculty at Michigan State University developed and manufactured a microscale heat exchanger from a zirconia composite. The microscale heat exchangers performance was analyzed with the aid of the testing apparatus built in this work. A mathematical model was also utilized to validate the experiment and testing device.

ACKNOWLEDGEMENTS

I would like to thank Dr. Craig W. Somerton for being my academic advisor and for never giving up on me. He was always there whenever I needed him. I would also like to thank my other committee members Dr. Patrick Kwon and Dr. Eldon Case for being on my panel. They were also responsible for the manufacturing of the microscale heat exchanger tested in this thesis. I would also like to acknowledge Professor Andre Benard for his help with the LabVIEW program used in this work. I would also like to thank Alan Lawrenz for his aid in the manufacturing of the flow rate measurement device.

I would also like to thank Nicole Aitcheson for her support and faith in me for completing this work. Last but not least I would like to thank my parents David and Sally Fickes for putting up with me and always pushing me through the six and a half years I spent at Michigan State University completing my Undergraduate and Graduate Degrees in Mechanical Engineering.

TABLE OF CONTENTS

LIST OF TABLES.. .vi

LIST OF FIGURES..vii

NOMENCLATURE..viii

Chapter 1
Introduction..1
1.1 Relevant Literature...1
1.2 Goals and Objectives...6

Chapter 2
Testing Device Fabrication..7
2.1 The Heat Exchanger..8
2.2 Thermocouples..9
2.3 The Test Channel...10
2.4 The Aluminum Billet.. 12
2.5 Reservoir Tanks.. 14
2.6 Silicone Heater.. 16
2.7 Submersible Pump.. 17
2.8 Flow Rate Measurement Device... 18

Chapter 3
Experimental Procedures...21
3.1 Experimental Test Run.. 21
3.2 Processing the Flow Rate 23

Chapter 4
Experimental Results...25
4.1 Determining Thermal Conductance..25
4.2 Error Analysis of Thermal Conductance..27
4.3 Fluid Mechanics...30

Chapter 5
Mathematical Model...32
5.1 Theoretical Thermal Conductance.. 32
5.2 Comparing $(UA)_{Exp}$ and $(UA)_{Th}$.. 35

Chapter 6
Conclusion...39
6.1 Discussion..39
6.2 Recommendations...41
6.3 Final Remarks..42

BIBLIOGRAPHY.. 43

APPENDIX A
LabVIEW Programs... 45

APPENDIX B
Voltage vs. Time Graphs for Determining Volume Flow Rate........................56

APPENDIX C
Excel Spreadsheet Containing Experimental Data and Calculations.................. 58

LIST OF TABLES

2.1 Microscale Heat Exchanger Zirconia Powder Information.......................8

2.2 Thermal Conductivity Values for Zirconia at Two Temperatures............. .9

3.1 Experimental Procedure Steps...23

4.1 Thermal Conductance Values..26

4.2 Volume Flow Rate Values...26

4.3 Uncertainty Values for Measured Parameters...................................29

4.4 Uncertainty Values for Each Test Run..29

4.5 Reynolds Number for Each Test Run..30

4.6 Hydrodynamic Entry Lengths for Each Test Run...............................31

4.7 Thermal Entry Lengths for Each Test Run......................................31

5.1 Theoretical Thermal Conductance Values.......................................35

LIST OF FIGURES

2.1 Testing Device Setup... 7

2.2 Microscale Heat Exchanger Next to a Penny.................................... 8

2.3 Sketch of Bottom View of Testing Channel.....................................12

2.4 Aluminum Billet.. 13

2.5 Sketch of Reservoir to Illustrate Modifications..................................15

2.6 Exit Reservoir Tank...16

2.7 Testing Device...17

2.8 Flow Rate Measurement Device...19

4.1 Thermal Conductance vs. Volume Flow Rate for Four Heater Settings.......27

5.1 Mathematical Model Alongside Thermal Circuit................................32

5.2 Nusselt Number Obtained from Entry Length Solutions for Laminar Flow in a Circular Tube...34

5.3 $(UA)_{Exp}$ and $(UA)_{Th}$ vs. Volume Flow Rate for Heater Variac Setting 30.....36

5.4 $(UA)_{Exp}$ and $(UA)_{Th}$ vs. Volume Flow Rate for Heater Variac Setting 50.....36

5.5 $(UA)_{Exp}$ and $(UA)_{Th}$ vs. Volume Flow Rate for Heater Variac Setting 60.....37

5.6 $(UA)_{Exp}$ and $(UA)_{Th}$ vs. Volume Flow Rate for Heater Variac Setting 70.....37

B.1 Voltage vs. Time Graph to Obtain Volume Flow Rate..........................57

B.2 Voltage vs. Time Graph to Obtain Volume Flow Rate..........................57

NOMENCLATURE

A	Area
A_{HE}	Area of Heat Exchanger
A_w	Area of Water
C	Celsius
D	Diameter
D_{HE}	Diameter of Heat Exchanger Channel
$d(UA)$	Uncertainty of Thermal Conductance
fn	Function
Gz	Graetz Number
h_w	Convection Coefficient of Water
I	Amps
In	Inches
InH_2O	Inches of Water
K	Kelvin
k_{HE}	Thermal Conductivity of Heat Exchanger
k_w	Thermal Conductivity of Water
L	Length
L_{HE}	Length of Heat Exchanger Channel
mL	Milliliter
Nu_D	Nusselt Number
Pr	Prandtl Number
$\dot{Q}$	Heat Conduction
R_{Cond}	Conductive Resistance
R_{Conv}	Convective Resistance
R_{Tot}	Total Thermal Resistance
Re_D	Reynolds Number
T_{in}	Inlet Temperature
T_{out}	Outlet Temperature
T_w	Water Temperature
T_3	Temperature of Bottom of Heat Exchanger
U	Overall Heat Transfer Coefficient
UA	Thermal Conductance
UA_{Exp}	Experimental Thermal Conductance
UA_{Th}	Theoretical Thermal Conductance
v	Velocity
V	Volt
$\dot{V}$	Volume Flow Rate
W	Watts
ΔT	Change in Temperature
μ	Dynamic Viscosity
ρ	Density

Chapter 1

Introduction

This study involved the manufacturing, testing, and analysis of a device for the testing of a microscale heat exchanger. The device simulated heat transfer from a computer chip by a single phase microscale heat exchanger. Water was used as the cooling fluid. The motivation of this thesis was to develop the concept of liquid cooled microprocessor chips. Faculty at Michigan State University developed and manufactured a microscale heat exchanger from a zirconia composite. The goal of this work was to test and analyze the functionality of this microscale heat exchanger. A mathematical model was also investigated to ensure the validity of the experiment.

1.1 Relevant Literature

Technology has been growing at an exceptional rate. New and better technological findings, concepts, and products have developed all across the world. Not only has technology become better and faster, but it has become exceptionally smaller. As technology has become smaller, it brought conventional concepts into a whole new regime. Conventional concepts, such as conductive heat transfer, are questioned as the length scales decrease from macro to micro and now even into nano regimes.

In 1994, Tien and Chen [1] found challenges in conventional theories, experiments, and engineering applications in microscale conductive heat transfer. They addressed these challenges and proposed new ideas and specific directions to follow for future research in the field of microscale heat conduction. Based on the characteristic lengths involved in the conduction process at this scale, two microscale heat conduction regimes were proposed to involve the classical and the quantum size effects.

Eight years later in 2002, Chen and Yang et al. [2,3] stated that heat conduction in micro- and nanoscale as well as in ultra-fast processes may deviate from the conventional Fourier's Law of heat transfer. They believed this was due to boundary and interface scattering and the finite relaxation time of the heat carriers. Therefore they presented a derivation of a new type of heat conduction equations they called the ballistic-diffusive equations. These equations were appropriate for describing transient heat conduction from nano to macroscale, and were derived from the Boltzmann equation under the relaxation time approximation.

Although nanotechnology has been a great focus in the engineering field for a few years now, technology at the microscale level is still being researched in certain areas. There is a great need for the development of liquid cooled microscale heat exchangers. Microprocessor chips have become smaller and faster, thus heat is being generated from a much smaller surface area. There is a need for a way to effectively cool these microprocessor chips. Computers today are fan cooled. A more effective cooling method would be liquid cooling. Liquids have a higher thermal capacity than gases and are more efficient as a cooling aid. A great example is modern snowmobiles. As technology has advanced, snowmobile engines that used to be fan cooled are now running more efficiently now that they are liquid cooled.

In order to develop a liquid cooled microscale heat exchanger, an understanding of what is hydrodynamically and thermally happening in this regime must be considered. Tuckermann and Pease [4,5] performed some of the earliest research on microscale fluid flow and heat transfer in the early 1980s. It was realized that electronic chips could be cooled by the means of forced convection flow of water through microchannels fabricated in the silicon wafer or in the circuit board on which the wafers were mounted. The first findings presented that at a power density of 790 W/cm^2, they achieved a temperature rise of 71 °C from inlet to outlet. Later a maintained surface temperature of less than 130 °C was achieved while the dissipated heat flux was on the order of 1.3 X 10^7 W/m^2.

Many have followed Tuckermann and Pease and have conducted their own experiments on fluid flow and heat transfer in microchannels. Experiments began to focus on size effects of hydraulic diameters on forced flow convection of fluid through microchannels. In 1994 Wang and Peng [6] experimentally investigated the single phase forced convective heat transfer of water/methanol flowing through rectangular cross-sectioned microchannels. It was found that liquid convection characteristics in the micro regime were quite different than the conventional cases. It was found that at Reynolds numbers of 1000-1500, the fully developed turbulent convection regime was initiated. Also, the mixing region from laminar to turbulent was found to begin for Reynolds number less than 800.

Later in 1994 Peng, Peterson, and Wang [7] furthered the studies using water for forced flow convection through rectangular microchannels. It was determined that varying the hydraulic diameters of the microchannels directly affected the flow and heat transfer regimes. Experiments confirmed that the upper bound of laminar heat transfer occurred at Reynolds numbers of 200-700. The fully developed convective heat transfer regime occurred at Reynolds numbers of 400-1500.

In 1996 Peng and Peterson [8] completed more experiments. This time a binary water-methanol was used as the cooling liquid for forced flow convection through rectangular microchannels. It was observed that laminar heat transfer ceased at lower Reynolds numbers of 70-400, and that at Reynolds numbers of 200-700 were in the fully developed turbulent heat transfer regime. It was also found that the transition Reynolds number reduced as the dimensions of the microchannels decreased. The range of the transition regime was also observed to become smaller.

Just recently in 2002, Gao et al. [9] experimented with two-dimensional microchannels. The testing device built allowed a range in the height of the microchannel from 0.1-1.0 mm while the width remained constant at 25 mm. It was found that the classical laws of hydrodynamics and heat transfer agreed with experimental measurements of the overall friction factor and local Nusselt number when the height of the microchannel was greater than 0.4 mm. A decrease of the Nusselt number was found at lower microchannel heights. It was found that the transition to turbulence was not affected by the size of the channel and occurred at Reynolds numbers in the range of 2500-4000.

There have been many experiments conducted on microscale heat exchangers. The flow and heat transfer regimes vary with each study, depending on the hydraulic diameters and the fluid used for convective cooling. Knowledge of fluid flow and heat transfer phenomena in microchannels is still developing. Boiling in microchannels and improving mathematical models to coincide with experimental data have also become a focus in this area.

Hapke et al. [10] proposed that the for boiling incipience have changed in microchannels compared to macroscale evaporator channels. A technique to measure the wall temperature of an evaporator channel in a quasi-continuous and non-contact manner was proposed. From this, the local heat transfer coefficient could be calculated. The method was used to investigate the onset of nucleate boiling in microchannels.

Kim and Kim [11] calculated analytical solutions for the velocity and temperature profiles in a microchannel heat sink. The microchannel heat sink was modeled as a fluid saturated porous medium. The two-equation model for heat transfer and the modified Darcy model for fluid flow were used to obtain the analytical solutions. It was shown that the porous medium model predicted the volume average velocity and temperature distributions quite well. Kim and Kim [11] compared analytical solutions to findings from Tuckermann and Pease [1]. The model was also successful for thermal optimization and prediction of the thermal resistance of the microchannel heat sink.

Babin et al. [12] combined an analytical and experimental investigation on performance limitations and operating characteristics of micro heat pipes. For operating temperatures between 40 °C and 60 °C the experimental maximum heat transport capacity was accurately predicted for steady state cases. Transient cases were not investigated. Babin claimed that there are several factors that affect both steady state and transient cases and further studies must be explored.

Jayan [13] explored factors that influence the forced flow convective heat transfer of water through microchannels. These factors included the velocity of the water, hydraulic diameter of the channel, number of channels, the inlet water temperature, and the wall temperature. The hydraulic diameter was optimized for the maximum heat flux used in the experiment. It was found that the optimum heat transfer rate, heat flux, heat transfer coefficient, and Nusselt number increased almost linear with the velocities tested.

1.2 Goals and Objectives

- Design and manufacture a testing apparatus for the microscale heat exchanger.
- Experimentally analyze the performance of the microscale heat exchanger for various power supplies and volume flow rates.
- Evaluate a mathematical model of the microscale heat exchanger.
- Compare the experimental data with the mathematical model to validate the experiment.
- Make recommendations to enhance the manufacturing of microscale heat exchangers and testing devices.

Chapter 2

Testing Device Fabrication

There are two main concerns that need to be addressed in order to simulate the heat transfer from a computer chip by the microscale heat exchanger; supplying the heat to the heat exchanger and moving the cooling liquid through the heat exchanger. Once a test was in progress certain data must be collected in order to properly analyze the heat exchanger. The three main measurements are the operating temperatures, the power supplied to the heat exchanger, and the mass flow rate of the cooling water. This chapter focuses on the manufacturing aspects of the testing device so that the microscale heat exchanger can be analyzed and assessed.

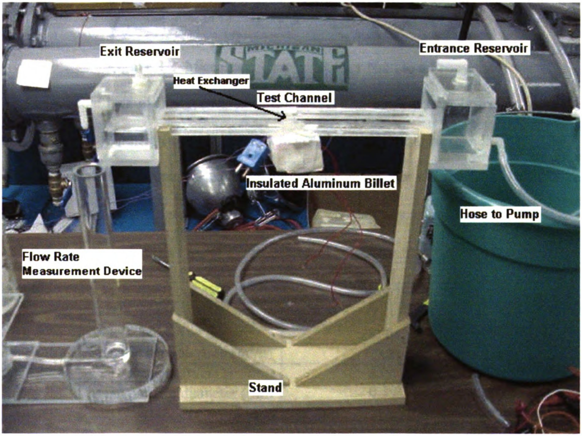

Figure 2.1 Testing Device Setup.

2.1 The Heat Exchanger

The microscale heat exchanger was designed and manufactured by members of the College of Engineering at Michigan State University. A picture of one such heat exchanger can be seen in Figure 2.2. The heat exchanger that was tested in this work has the dimensions of 16.9 mm by 2.4 mm by 5.2 mm (width by height by depth). There are six cylindrical channels with a diameter of 0.5 mm through the heat exchanger with lengths equal to the depth of the device (5.2 mm).

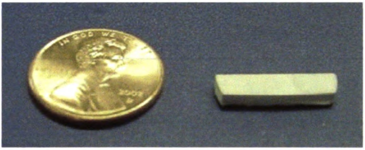

Figure 2.2 Microscale Heat Exchanger Next to a Penny.

The microscale heat exchanger tested in this thesis was made primarily from a zirconia powder. The compostion along with other material properties can be seen in Table 2.1.

Table 2.1 Microscale Heat Exchanger Zirconia Powder Information. [14]

Materials	TZ-3YS (partially stabilized)
Y_2O_3 (mol %)	3
Y_2O_3 (wt %)	5.15±0.20
Al_2O_3 (wt %)	≤0.1
SiO_2 (wt %)	≤0.02
FeO_2 (wt %)	≤0.01
Na_2O (wt %)	≤0.04
Specific surface Area (m^2/g)	7±2
Density (g/cm3)	6.05
Mean particle diameter (μm)	0.59

This work did not deal with the manufacturing of the microscale heat exchanger, rather its performance. The most important thermo physical property of the heat exchanger for this thesis was its thermal conductivity. Table 2.2 shows the thermal conductivity of ZrO_2, the main ingredient in the heat exchanger. Since the composition of the heat exchanger was mostly ZrO_2, this work considered the microscale heat exchanger to have a thermal conductivity of 1.675 W/(mK).

Table 2.2 Thermal Conductivity Values for Zirconia at Two Temperatures.[14]

Material	Thermal Conductivity W/(mK)
ZrO_2	1.675 (at 100°C) 2.094 (at 1300°C)

2.2 Thermocouples

There were five thermocouples fabricated for this thesis work. The thermocouples that were fabricated are type T thermocouples. The positive lead was made of copper and the negative lead was made of constantan. The method used to construct the type T thermocouples was mechanical tying. Four of the five thermocouples had only approximately 1.5 mm of insulation stripped off of the wires. These were for measuring the temperature of the water in the testing channel that has a height of only 2.4 mm. Three of these thermocouples were wired together in parallel so they could measure an average exit temperature. The fifth thermocouple had approximately 8 mm of insulation stripped of the wires. This thermocouple measured the temperature of the bottom of the microscale heat exchanger. All thermocouples were connected to type T *Omega* Microprocessor Digital Thermometers for recording temperatures. More detail on where these thermocouples were placed is discussed in Sections 2.3 and 2.4.

2.3 The Test Channel

It is obvious that for a liquid cooled heat exchanger there must be a channel, duct, tube, etc. to contain the flow and supply it to the heat exchanger. These channels must be watertight. The testing device was therefore constructed of 9 mm thick acrylic sheet stock, also known as Plexiglas. Acrylic was easy to cut, but difficult to produce nice finished cuts. A table saw was used to cut the acrylic and it was a challenge to not leave saw marks on the finished cut edge. As a result of this, all acrylic cuts on the table saw were oversized. These oversized parts were then easily machined to their corresponding dimensions on a mill. The mill leaves the acrylic with a nice finished edge, which was essential when it came time to fabricate the parts together to form the channel.

The microscale heat exchanger was approximately a rectangular prism; hence the channel that was manufactured had a rectangular cross section. This cross section had the dimensions of 16.9 mm by 2.4 mm corresponding to the width and the height of the heat exchanger. The length of the channel was 296 mm. The heat exchanger was in the middle of this channel resulting in 145.4 mm of channel before the entrance of the heat exchanger, and 145.4 mm after. This distance was nearly 28 times the depth of the microscale heat exchanger.

The channel consisted of five separate acrylic parts. The top piece was 296 mm by 16.9 mm. The bottom of the channel consisted of two pieces of acrylic, each 145.4 mm by 16.9 mm. These dimensions allowed for a 5.2 mm gap (the depth of the heat exchanger) in the middle of the bottom of the channel. This gap allowed for an aluminum billet to make contact to the bottom of the heat exchanger, which conveyed the heat to the heat exchanger. This is discussed more in Section 2.4. Both sides of the channel had the same dimensions, 296 mm by 20.4 mm. The 20.4 mm dimension was determined from the height of the heat exchanger, 2.4 mm, plus two thicknesses' of acrylic, 9.0 mm each. This was to ensure fabricating a channel with even edges on the exterior.

To manufacture a perfect rectangular box with acrylic sheet stock, two pieces were put together at a time. The best way was to lightly clamp the two pieces together making sure they were flush on all ends and edges, and also checking to make sure they were at 90 degrees from each other. Once in place the two parts were easily bonded together with methylene chloride. The methylene chloride was applied with a syringe along the edges of the surface where the two pieces of acrylic were in contact. The methylene chloride wicked into the acrylic and bonded the two parts together. Once the methylene chloride was applied, the clamps were tightened in order to ensure a good watertight bond. This method of bonding acrylic with methylene chloride was used for all testing parts, where applicable, in this work.

When the duct was completely bonded together five 1 mm holes were drilled into the duct. These holes permitted the thermocouples to be inserted into the channel for the temperature measurements. Four of the holes were drilled into the bottom of the channel. The first hole was drilled into the center of the bottom of the channel 47 mm from the center edge. The center edge was the edge in the middle of the duct where the 5.2 mm gap was located. This upstream thermocouple would measure the inlet temperature.

Figure 2.3 shows a view of the bottom of the testing channel. The dots are the thermocouple holes.

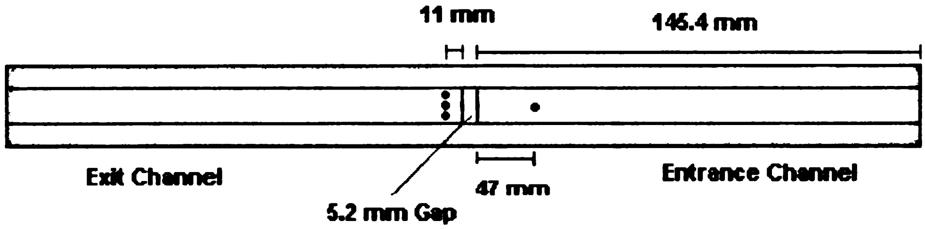

Figure 2.3 Sketch of Bottom View of Testing Channel. (not to scale)

The next three holes were drilled out 11 mm from the center edge on the other side of the 5.2 mm gap. These holes would be used for the thermocouples that measured the outlet temperature. These three thermocouples were wired in parallel to obtain an average temperature across the width of the channel. The first of these three holes was drilled in the center of the channel. The next two were equidistant from the center hole and the edge of the channel. The fifth and final hole was drilled in one of the sides of the channel. The hole was to be 9mm from the bottom at the mid point of the length of the channel. The thermocouple inserted into this hole measured the temperature of the bottom of the heat exchanger.

2.4 The Aluminum Billet

The aluminum billet's purpose was to act as a computer chip. The bottom of the billet was heated with a rubber silicone heater, and heat was conducted to the top of the billet, which was in contact with the bottom of the heat exchanger. The billet was machined out of cylindrical stock 2024-T351 aluminum with a 25.4 mm diameter. The bottom of the microscale heat exchanger is 16.9 mm by 5.2 mm, which provided the required dimension of the aluminum billet. The 25.4 mm diameter cylinder was altered on a mill to a 16.9 mm by 5.2 mm by 15 mm rectangular prism, see Figure 2.4. At this point there was a rectangular prism on the end of a cylindrical rod. The rod was then cut on a drop saw to leave 12.7 mm of cylinder plus the 15 mm length of the rectangular prism.

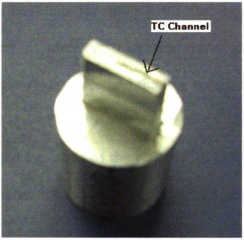

Figure 2.4 Aluminum Billet.

The last task on the aluminum billet was to cut a thin channel on the top of the rectangular prism (farthest from the cylindrical end) halfway across, see Figure 2.4. This channel was cut with a *Dremel* and its purpose was for a thermocouple lead to lie in. Solid contact between the bottom of the heat exchanger and the top of the billet was essential. Temperature was measured between these two and the thickness of the thermocouple wire between the two would not provide good surface contact. A groove was made to allow the thermocouple wire to be flush and enhance a good contact surface between the billet and the microscale heat exchanger.

The aluminum billet and the microscale heat exchanger were installed into the testing channel. The top of the heat exchanger was first applied with cyanoacrylate glue. The heat exchanger was then inserted into the 5.2 mm gap in the bottom of the channel joining the glued topside of the heat exchanger to the underside of the top of the channel.

With the heat exchanger in place, the aluminum billet was mounted. The cyanoacrylate glue was applied around the edges of the rectangular prism where it came into contact with the edges around the 5.2 mm gap. Before the aluminum billet was pushed into contact with the bottom of the heat exchanger, a thermocouple was inserted to the previously drilled side hole and into the groove on the top of the billet. This thermocouple was also glued in place with cyanoacrylate glue. The other four thermocouples could now be glued into place into the four remaining holes located at the bottom of the channel. The tips of the thermocouples were centered in the channel, equidistant from the bottom and top walls of the channel. All five thermocouples were set with cyanoacrylate glue. When the glue set, a ball of glue was set on the wires where they penetrate the channel on the outside with a hot glue gun. This would ensure that the wires would not get pulled out of place. The testing channel was now complete.

2.5 Reservoir Tanks

To move water through the testing channel a flow system was designed and built. Reservoir tanks for the cooling water were located at each end of the testing channel. These reservoir tanks were made out of acrylic sheet stock in the same manner that the testing channel was fabricated. These tanks have outside dimensions of 66 mm by 70 mm by 85 mm.

Once completed the reservoir tanks needed to be slightly modified. Two holes were drilled and tapped to fit a ¼" by ¼" nylon hose barb to MIP elbow in each of the two reservoir tanks. Each tank had one elbow installed on the top, (one of the 66 mm by 70 mm sides). These top elbows could be positioned anywhere on the top surface since their purpose was to relieve pressure from the reservoir tanks and allow them to fully drain once full of water. The elbow on the top of the entrance reservoir had a six inch hose attached to it. Figure 2.5 shows a sketch of the top view and front view of the reservoir and displays locations of modifications.

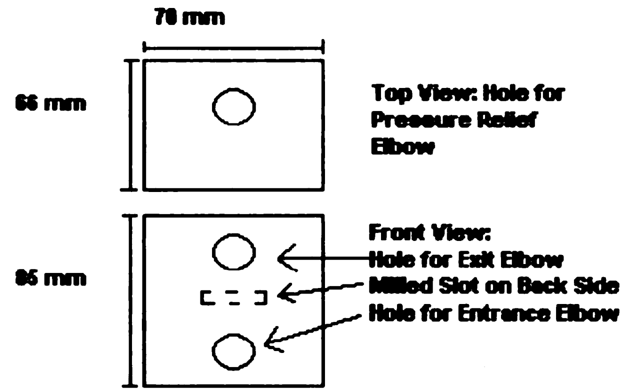

Figure 2.5 Sketch of Reservoir to Illustrate Modifications. (not to scale)

The entrance reservoir tank had the second elbow installed on one of the 85 mm by 70 mm sides. The hole for this elbow was drilled in the center towards the bottom of the reservoir tank. The exact position was arbitrary. When screwing in the elbow it was positioned specifically so that the barb was pointing down. This is where the water entered the reservoir tank.

The exit reservoir tank had the second elbow installed on one of the 85 mm by 70 mm sides. The hole for this elbow was drilled in the center towards the top of the reservoir tank. The exact position was arbitrary. When screwing in the elbow it was positioned specifically so that the barb was pointing down. This is where the water exited the reservoir tank. To better understand what these reservoir tanks look like, see Figure 2.6.

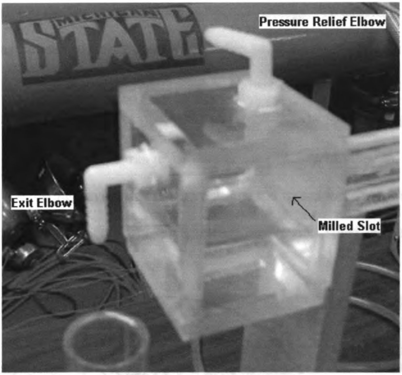

Figure 2.6 Exit Reservoir Tank.

Both tanks then had a slot milled into the center of the 85 mm by 70 mm side opposite the exit or entrance elbow. This slot was slightly oversized compared to the 16.9 mm by 2.4 mm channel area. The testing channel was bonded to the reservoir tanks around these slots with methylene chloride in the same manner as previously described. This provided the path to convey the water from one reservoir tank into the testing channel, and then back to the other reservoir tank.

2.6 Silicone Heater

The heat supplied to the bottom of the aluminum billet was from a 1" by 1" Omega flexible silicone rubber heater, rated for a maximum of 115 VAC. Both the heater and the aluminum billet were surrounded by standard 2" foamular house insulation. In order to complete a variety of tests on the microscale heat exchanger, it was desirable to supply the heater with a range of power settings. To accomplish this the silicone heater was connected to a *Powerstat* variable autotransformer, or variac. This variac takes in 120 V from a standard wall plug, and gives out anywhere from 0-120 V, depending on its setting. By adjusting the setting on the variac, the heater could receive a variety of voltages resulting in a range of power supply. With this in place the manufacturing of the testing device was complete. A stand to support the testing device was also fabricated out of wood. The final testing device and stand can be seen in Figure 2.7.

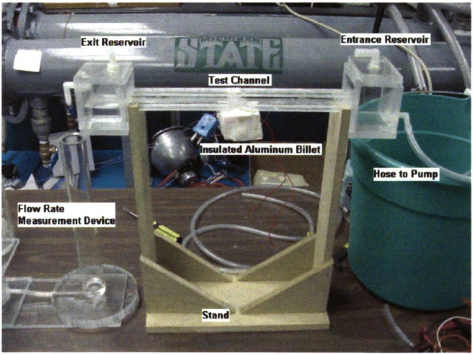

Figure 2.7 Testing Device.

2.7 Submersible Water Pump

A submersible water pump by *Teel* was used to move water through the channel. The pump was rated for 115V, 60Hz, and 2.2A. The pump was completely submersed in a 4.5 gallon bucket of water. It was desirable to be able to test the microscale heat exchanger at a range of flow rates. Therefore the pump was plugged into another *Powerstat* variable autotransformer, or variac. This variac takes in 120V from a standard wall plug, and gives out anywhere from 0-120V, depending on its setting. By adjusting the setting on the variac, the submersible pump would receive a range of power resulting in various flow rates through the testing channel. A hose connected the outlet of the submersible pump to the entrance elbow on the entrance reservoir.

2.8 Flow Rate Measurement Device

The flow rate was adjustable so there had to be a means of measuring the various flow rates. To complete this task a flow rate measuring apparatus was constructed, see Figure 2.8. This device was made from acrylic. It consists of two cylinders; one stands 11" tall with an inner diameter of 1.1875', and the other stands 3" tall with and inner diameter of 2.25". The shorter cylinder had a cover put on the top; again all bonding was done with methelyne chloride. A pressure tap was installed in the center of the cover. The two cylinders also had pressure taps inserted into the sides facing each other towards the bottom of each cylinder. These two taps were connected with a hose.

Water was then added to the uncovered tall cylinder. Due to gravity some of the water would flow out of the tall cylinder, through the connecting tube, over to the short cylinder until the water levels were even. The water levels would even out because of the open tap on the covered cylinder. Once the water levels were even, a hose was attached to the tap on the top of the covered cylinder. The other end of this hose was connected to a *Validyne* pressure transducer with an Mp value of 0.2369448152 InH_2O/V. The pressure transducer was then connected to a *Hewlett Packard* 3852A Data Acquisition Control Unit, which in turn was directly linked to a personal computer with a built in analog to digital board.

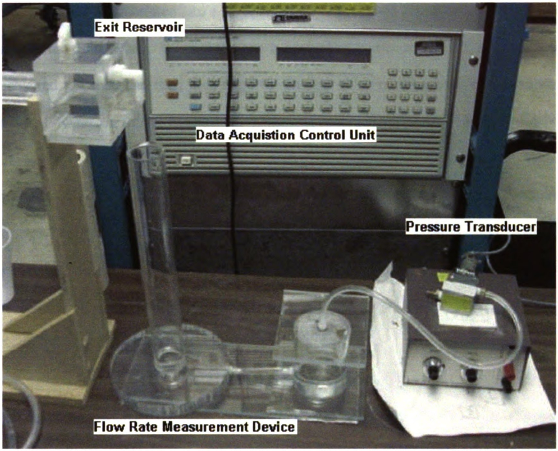

Figure 2.8 Flow Rate Measurement Device.

A program was written in LabVIEW on the computer to acquire transient data in volts. This LabVIEW program can be found in Appendix A. The flow rate measuring apparatus was now complete. When water exited the reservoir tank out of the elbow, it would drip into the uncovered tall tube. The water level in this tube would then rise. The water would not level out in the covered tube because the pressure tap was covered with a tube. Instead, the air pressure would rise in the short tube due to the added pressure on the water level in the tall tube. This pressure rise would be transmitted from the pressure the water level in the tall tube. This pressure rise would be transmitted from the pressure transducer to the PC by means of the *Hewlett Packard* 3852A Data Acquisition Control Unit. The LabVIEW program would acquire this data recording the voltage and time. This data could be translated into a graph of increasing voltage versus time. The slope of this line has units V/sec. When this slope is multiplied by the cross sectional area of the uncovered tall tube and then multiplied by the Mp value of the pressure transducer, a volume flow rate in In^3/sec is acquired. (This will be discussed more in Section 3.2.)

Chapter 3

Experimental Procedures

3.1 Experimental Test Run

A simple experimental procedure for testing the microscale heat exchanger was developed. Step one involved turning on both variacs, the silicone heater and the submersible pump. The heat exchanger was tested for various power levels. For each of the power levels for the heater, a range of volume flow rates were explored. Again, these variations for power and flow rate were accomplished by simply adjusting the variac controller. With the appropriate power setting for a particular test run, the slowest volume flow rate was tested first. The slowest volume flow rate was determined by setting the variac to 50 on its range from 0 to 120. This was the lowest setting in which the submersible pump would operate.

As the pump began, water would begin to fill the entrance reservoir tank. When this reservoir was full the six inch hose attached to the elbow on the top of the tank was clamped. Now water was forced to flow through the testing channel. The water flowing through the heat exchanger and into the exit reservoir tank would eventually reach a level so it would flow out the exit elbow and into a bucket. The elbow on the top of the exit reservoir was always open to the ambient. All three temperature measurements were then monitored. The inlet temperature was constant for each test run. The heat exchanger temperature and the exit temperature were closely monitored. When these two temperatures became steady state, all three temperature measurements were recorded.

To measure the flow rate, the LabVIEW program was started, and the flow rate measuring apparatus was set under the exit elbow so the water flowing out would now drip into the large uncovered cylinder. As the water level rose in that cylinder, the pressure transducer sensed the increased air pressure in the covered cylinder. The LabView program via the *Hewlitt Packard* 3852A Data Acquisition Control Unit was constantly recording this increase in voltage. The DMM was monitored so that the flow rate measuring apparatus could be pulled away from the water flow before a value of 10V was reached. (This was done because the pressure transducer used was rated for ±10V.) The LabVIEW program was then terminated. The tube from the pressure transducer to the pressure tap on the covered cylinder was then pulled off of the pressure tap; this was done so the water levels in each cylinder would become level again. When they were level, the hose was reattached and the flow rate was measured a second time. The last step in a test run was to measure the voltage and current being supplied to the heater. This was done with an HHM59 Clamp Meter by Omega.

The variac supplying the submersible pump was then turned up in order to increase the flow rate. The system was allowed to steady, the temperatures were then recorded, the flow rate was measured twice, and the voltage and current supplied to the heater was recorded in the same fashion. Test runs were performed for heater variac settings of 30, 50, 60, and 70, and for flow rate variac settings of 50, 60, 65, 70, 80, 90, and 100. The inlet water temperature was at room temperature, which varied from 17.6-25.4 °C day to day. As the pump operated it would transfer heat to the water. Ice was added to the bucket to maintain a relatively constant water temperature. A table of experimental procedure steps is in Table 3.1.

Table 3.1 Experimental Procedure Steps.

Step	Procedure
1	Turn on pump and heater variacs.
2	Set variac dials to desired level.
3	Clamp 6" hose on entrance reservoir when full of water.
4	Let temperatures reach steady state.
5	Record inlet, outlet, and heat exchanger temperatures.
6	Start LabVIEW program.
7	Place Flow Rate Measurement Device (FRMD) under exit elbow.
8	Remove FRMD before 10 V is reached on the DMM.
9	End LabVIEW program.
10	Remove hose from FRDM and let the two water levels become equal.
11	Reattach hose and repeat steps 6-10.
12	Measure heater voltage and current with HHM59 Clamp Meter.
13	Process flow rate data (see Section 3.2).
14	Repeat steps 2-13 for next test.

3.2 Processing the Flow Rate

The data acquired from the LabVIEW program was opened in Microsoft Excel. The data was collected as two columns, time and voltage. First, all unnecessary data points in the Excel file were deleted. Since the LabVIEW program was started before the flow rate measurement device was under the exit elbow of the test apparatus, and also continued after it was pulled away from the exit elbow, data before and after the test water was flowing into the tall tube of the flow measurement device was unwanted and deleted.

Second, the time needed to be adjusted. The program kept a continuous time so all of the time points had the initial time subtracted from their values. This resets the first data point to time zero and counts from there. Recorded time was also in milliseconds so all times were then multiplied by 1000 to become seconds.

The two columns of data were then plotted as voltage versus time in a scatter plot on Excel. Flow rate was constant and, as expected, data points formed a linear line. A linear trend line was then applied and the equation was displayed. Once the slope of this line was known, the volume flow rate could easily be calculated. A sample graph of Voltage vs. Volume Flow Rate for a test run is in Appendix B.

The slope of the linear lines obtained from the flow rate measurement device had the units of Volts/second. The pressure transducer used had an Mp value of 0.2369448151 InH_2O/Volt and the inner diameter of the tall tube of the flow rate measurement device was 1.1875". These three parameters are multiplied together to obtain the volume flow rate

$$\dot{V} = slope \times Mp \times A. \tag{3.1}$$

The units work out to give a flow rate in In^3/sec

$$\frac{In^3}{\sec} = \frac{Volts}{\sec} \times \frac{InH_2O}{Volts} \times In^2. \tag{3.2}$$

The volume flow rate was then converted from In^3/sec to mL/sec.

Chapter 4

Experimental Results

4.1 Determining Thermal Conductance

The performance of the heat exchanger was characterized by the overall thermal conductance of the heat exchanger, UA, where U was the overall heat transfer coefficient and A was the area. Heat conduction was defined as

$$\dot{Q} = UA\Delta T . \tag{4.1}$$

For this work, the thermal conductance was determined from the heater voltage measurement (V), the heater current measurement (I), and the temperature measurements with the equation

$$UA = \frac{V \times I}{T_3 - T_{water}} \tag{4.2}$$

where T_{water} was the average water temperature as it flowed through the heat exchanger and was approximated as the linear average of the inlet and outlet temperatures. T_3 was the temperature of the bottom of the heat exchanger. It should be noted that all calculations were performed on an Excel spreadsheet that includes all data taken; this spreadsheet is in Appendix C.

Table 4.1 shows the results of thermal conductance for all tests.

Table 4.1 Thermal Conductance Values.

Variac Flow Rate Setting	Thermal Conductance (UA) in W/K			
	Variac Heater Setting 30	Variac Heater Setting 50	Variac Heater Setting 60	Variac Heater Setting 70
50	0.07395349	0.08622951	0.10520776	0.12461538
60	0.0795	0.09187773	0.11105263	0.13076233
65	Not Tested	0.09831776	0.11579268	0.13254545
70	0.08712329	0.09924528	0.11943396	0.13468822
80	0.09636364	0.10734694	0.12212219	0.13787234
90	0.09492537	0.10066986	0.12534653	0.14019231
100	0.09784615	0.10364532	0.12787879	0.1415534

From the table it was clear to see a general trend, as the flow rate was increased for any of the power settings, the thermal conductance increased. This was expected that as flow rate increased the convective coefficient would increase resulting in an increase of thermal conductance. Volume flow rate values can be seen in Table 4.2 for all tests. Recall that these flow rates are the average of two flow rate measurements.

Table 4.2 Volume Flow Rate Values.

Variac Flow Rate Setting	Volume Flow Rate (mL/sec)			
	Variac Heater Setting 30	Variac Heater Setting 50	Variac Heater Setting 60	Variac Heater Setting 70
50	0.6181777	0.58549491	0.55517733	0.59022531
60	0.89469127	0.844592	0.81405939	0.84738723
65	Not Tested	1.40385467	1.40492976	1.37891254
70	1.99838035	2.07148658	2.08653786	2.08890306
80	2.39401407	2.41401078	2.4013247	2.43637268
90	2.56538368	2.54001152	2.52474522	2.56860896
100	2.6324694	2.61010749	2.61870823	2.66192691

Table 4.1 and Table 4.2 are displayed in the form of a graph of thermal conductance versus volume flow rate for each of the variac power settings in Figure 4.1.

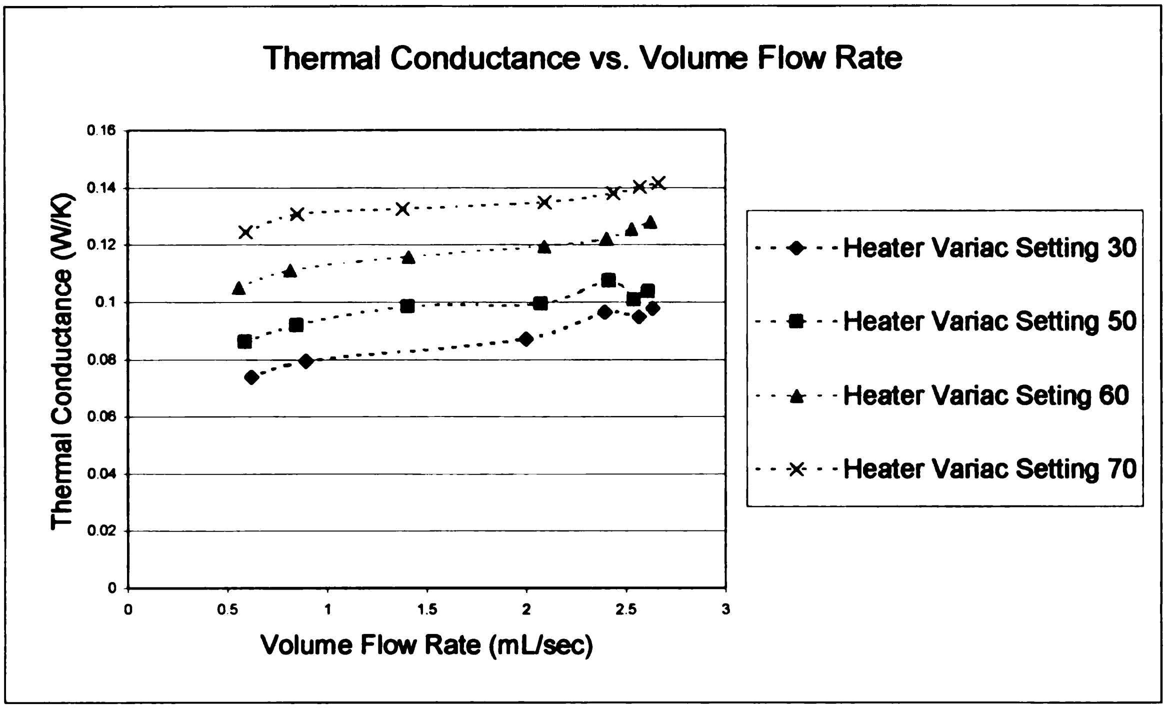

Figure 4.1 Thermal Conductance vs. Volume Flow Rate for Four Heater Settings.

The graph clearly shows an increase in thermal conductance as the volume flow rate was increased. It also illustrates that more power supplied to the heat exchanger resulted in a higher thermal conductance. The experimental uncertainty was considered in the next section.

4.2 Error Analysis of Thermal Conductance

The thermal conductance values UA were calculated from the experimental data. An error analysis was performed to calculate dUA to find the uncertainty of the thermal resistance analysis. The experimental determination of thermal conductance was based on all of the measurements taken to solve for UA. Recall Equation 4.2 for UA, there were five parameters that were experimentally measured: V, I, T_{in}, T_{out}, and T_3.

Differential calculus was used to determine the uncertainty for each test run that produced a UA value. Another form of Equation 4.2 produced the initial equation

$$UA = \frac{V \times I}{T_3 - \left(\frac{T_{out} + T_{in}}{2}\right)}. \tag{4.3}$$

Therefore UA was a function of voltage, current, and three different temperatures

$$UA = fn(V, I, T_3, T_{out}, T_{in}). \tag{4.4}$$

Differential calculus provides the equation for the uncertainty of the thermal conductance values

$$dUA = \left|\left(\frac{dU}{dV}\right)\right| dV + \left|\left(\frac{dU}{dI}\right)\right| dI + \left|\left(\frac{dU}{dT_3}\right)\right| dT_3 + \left|\left(\frac{dU}{dT_{out}}\right)\right| dT_{out} + \left|\left(\frac{dU}{dT_{in}}\right)\right| dT_{in} \tag{4.5}$$

where

$$\frac{dU}{dV} = \frac{2I}{2T_3 - T_{out} - T_{in}}$$

$$\frac{dU}{dI} = \frac{2V}{2T_3 - T_{out} - T_{in}}$$

$$\frac{dU}{dT_3} = \frac{-4VI}{(T_{out} + T_{in} - 2T_3)^2} \quad . \tag{4.6 - 4.10}$$

$$\frac{dU}{dT_{out}} = \frac{2VI}{(T_{out} + T_{in} - 2T_3)^2}$$

$$\frac{dU}{dT_{in}} = \frac{2VI}{(T_{out} + T_{in} - 2T_3)^2}$$

Plugging Equations 4.6 to 4.10 into Equation 4.5 results in the final equation for the uncertainty of the experimental parameter thermal conductance,

$$dUA = \left|\frac{2I}{2T_3 - T_{out} - T_{in}}\right| dV + \left|\frac{2V}{2T_3 - T_{out} - T_{in}}\right| dI + \left|\frac{-4VI}{(T_{out} + T_{in} - 2T_3)^2}\right| dT_3 + \left|\frac{2VI}{(T_{out} + T_{in} - 2T_3)^2}\right| dT_{out} + \left|\frac{2VI}{(T_{out} + T_{in} - 2T_3)^2}\right| dT_{in} \quad (4.11)$$

The uncertainty equation was applied to all test runs in this work. For a particular test run, the parameters V, I, T_{in}, T_{out}, and T_3 were plugged into Equation 4.11 as the appropriate values found in the experiment. dV, dI, dT_{in}, dT_{out}, and dT_3 were found to be the uncertainty of each particular measurement according to the instrument used to measure the parameter. Table 4.3 shows the uncertainty values for each parameter.

Table 4.3 Uncertainty Values for Measured Parameters.

Parameter	**Uncertainty**
Voltage	0.05 V
Current	0.005 A
Temperature	0.05 K
Temperature	0.05 K
Temperature	0.05 K

The uncertainty values for all test runs can be seen in Table 4.4. They all fall in a range of uncertainties of approximately 2.2-5.6%.

Table 4.4 Uncertainty Values for Each Test Run.

Variac Flow Rate Setting	Uncertainty Values (dUA)			
	Variac Heater Setting 30	Variac Heater Setting 50	Variac Heater Setting 60	Variac Heater Setting 70
50	0.04208058	0.02648092	0.02331527	0.02229257
60	0.04534063	0.02825247	0.0246362	0.02341288
65	Not Tested	0.03027793	0.02570942	0.02373822
70	0.049845	0.03057013	0.02653507	0.0241294
80	0.0553416	0.03312766	0.02714528	0.02471113
90	0.0544834	0.03101916	0.02787795	0.02513531
100	0.05622722	0.03195797	0.02845393	0.0253843

The uncertainty values are applied to an experimental thermal conductance vs. volume flow rate graph in the form of error bars in Section 5.2.

4.3 Fluid Mechanics

To analyze the fluid mechanics that was involved in the microscale heat exchanger the Reynolds number was calculated.

$$\mathrm{Re} = \frac{\rho v D}{\mu} \tag{4.12}$$

After calculating the Reynolds number for each test run it was clear that the flow through the channels was laminar. Table 4.5 displays the Reynolds number for each test run; flow was considered to be laminar if Re<2300. (There was no discontinuity in experimental data showing any changes in flow regimes (laminar, transition, and turbulent) to deviate from conventional concepts.) It should be noted that the volume flow rate was not exactly repeatable from one power setting to the next, for the same volume flow rate setting. Volume flow rate was measured for every test run for accurate analysis.

Table 4.5 Reynolds Number for Each Test Run.

Variac Flow Rate Setting	Reynolds Number			
	Variac Heater Setting 30	Variac Heater Setting 50	Variac Heater Setting 60	Variac Heater Setting 70
50	278.44798	255.44444	239.460826	239.037862
60	406.514802	369.645987	351.486248	343.186964
65	Not Tested	613.76973	599.161555	558.451661
70	919.016553	899.997449	889.847525	852.178219
80	1114.49706	1059.85955	1018.88549	1002.72725
90	1203.69475	1097.83708	1075.63023	1065.00703
100	1254.97099	1118.85575	1120.23948	1113.63052

Since the flow was clearly laminar the idea that the flow was not even fully developed was considered. After calculating the hydrodynamic and thermal entry length it was determined that both the velocity and thermal profiles were still developing through the entire heat exchanger. Recall that the length of the channels in the microscale heat exchanger was 5.2mm.

$$L_h = 0.05 \mathrm{Re}\, D \tag{4.13}$$

$$L_t = 0.05 \mathrm{Re}\, \mathrm{Pr}\, D \tag{4.14}$$

Table 4.6 Hydrodynamic Entry Lengths for Each Test Run.

Variac Flow Rate Setting	L_h: Hydrodynamic Entry Length (mm)			
	Variac Heater Setting 30	Variac Heater Setting 50	Variac Heater Setting 60	Variac Heater Setting 70
50	6.96119949	6.386111	5.98652066	5.97594656
60	10.1628701	9.24114967	8.7871562	8.57967409
65	Not Tested	15.3442432	14.9790389	13.9612915
70	22.9754138	22.4999362	22.2461881	21.3044555
80	27.8624266	26.4964889	25.4721373	25.0681812
90	30.0923687	27.445927	26.8907557	26.6251758
100	31.3742748	27.9713937	28.0059869	27.840763

Table 4.7 Thermal Entry Lengths for Each Test Run.

Variac Flow Rate Setting	L_t: Thermal Entry Length (mm)			
	Variac Heater Setting 30	Variac Heater Setting 50	Variac Heater Setting 60	Variac Heater Setting 70
50	45.0431374	42.9887448	40.8717725	43.6985116
60	65.0525313	61.9665291	59.9161033	62.7380088
65	Not Tested	103.024318	103.699886	102.090548
70	144.866877	152.243569	154.01036	154.63626
80	173.014524	176.980648	177.451644	180.330468
90	185.028948	186.904018	186.398651	190.093105
100	189.701415	192.429203	193.154491	196.96783

Chapter 5

Mathematical Model

5.1 Theoretical Thermal Conductance

The thermal conductance of the microscale heat exchanger was experimentally determined as well as its uncertainty. For the purpose of comparison, the heat exchanger was analyzed mathematically in order to obtain a theoretical thermal conductance. A thermal circuit analysis was used and can be seen in Figure 5.1. Tw was the linear average of the inlet and outlet water temperatures and T3 was the temperature of the bottom of the heat exchanger.

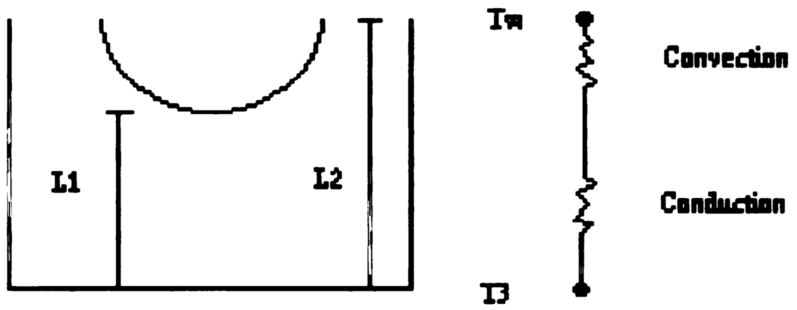

Figure 5.1 Mathematical Model Alongside Thermal Circuit.

Figure 5.1 shows a section of the microscale heat exchanger. There are six channels through the heat exchanger. The picture shows just the bottom half of one of the channels. On the sides of the channel, the picture was cut off at the mid point between the next channels on either side. L1 (0.95 mm) was the distance between the bottom of the heat exchanger and the bottom of the channels. L2 (1.2 mm) was the distance between the bottom of the heat exchanger and the center of the channels.

Theoretical thermal conductance was determined from the mathematical model using the thermal circuit model with the total thermal resistance as,

$$UA_{Th} = \frac{1}{R_{Tot}} \tag{5.1}$$

where,

$$R_{Tot} = R_{Cond} + R_{Conv}\,. \tag{5.2}$$

The total thermal resistance was the sum of the conduction resistance and the convection resistance. R_{Cond} was,

$$R_{Cond} = \frac{L_{HE}}{k_{HE} \times A_{HE}} \tag{5.3}$$

$$L_{HE} = \frac{L1 + L2}{2} \tag{5.4}$$

where L_{HE} was the length of the heat exchanger along the conduction line, k_{HE} was the thermal conductivity of the heat exchanger (1.675 W/(mK)), and A_{HE} was the area of the bottom of the heat exchanger.

R_{Conv} was,

$$R_{Conv} = \frac{1}{h_w \times A_w} \tag{5.5}$$

$$h_w = \frac{Nu \times k_w}{D_{HE}} \tag{5.6}$$

$$A_w = \frac{1}{2}\pi D_{HE} L_{HE} \tag{5.7}$$

where h_w was the convection coefficient of the water, and A_w was the area of the water. The convection coefficient could not be solved for until the Nusselt number was determined.

Equation 5.8 is for the Nusselt number for a constant surface temperature correlation.

$$Nu_D = 1.86\left(\frac{\mathrm{Re}_D \mathrm{Pr}}{L/D}\right)^{1/3} \tag{5.8}$$

The case at hand had a constant surface heat flux however. Therefore the aid of Figure 5.2 was induced into the equation.

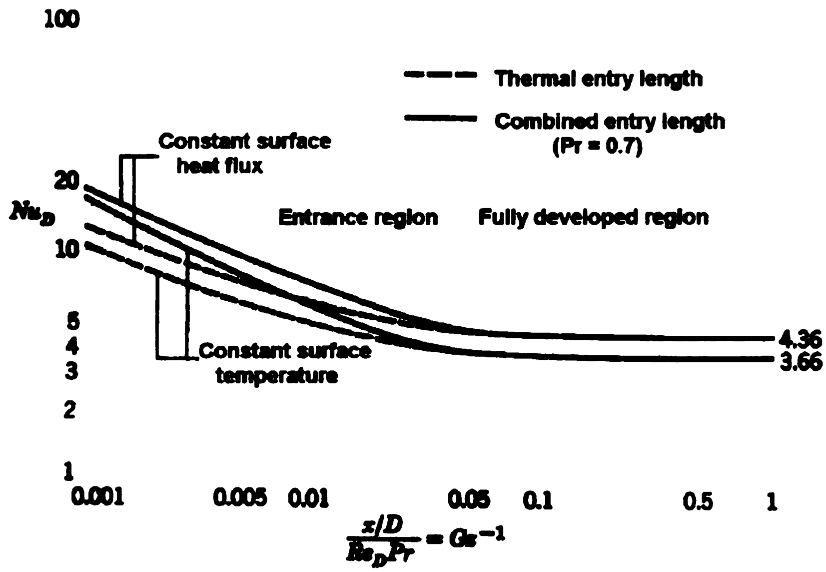

Figure 5.2 Nusselt Number Obtained from Entry Length Solutions for Laminar Flow in a Circular Tube. [15]

The two lines graphed are for a constant surface temperature and a constant surface heat flux. These lines are parallel when the inverse Graetz number is larger than 0.05. Before that point the two lines are very close to parallel but are not exact. For the approximation of the mathematical model it was assumed that these two lines were parallel throughout the entire graph. Therefore Equation 5.8 was multiplied by 4.36/3.66 in order to obtain an equation for Nu_D with a constant heat flux.

Table 5.1 gives all of the theoretical values of the thermal conductance for each test run.

Table 5.1 Theoretical Thermal Conductance Values.

Variac Flow Rate Setting	Theoretical Thermal Conductance (UA_{Th})			
	Variac Heater Setting 30	Variac Heater Setting 50	Variac Heater Setting 60	Variac Heater Setting 70
50	0.09956992	0.09902551	0.09851778	0.09893287
60	0.10283429	0.10228556	0.10194485	0.10215209
65	Not Tested	0.1064816	0.10644974	0.10619262
70	0.10923873	0.10943285	0.10945926	0.10938201
80	0.11055729	0.11055039	0.11046595	0.1105112
90	0.11105187	0.11088916	0.11082668	0.11089945
100	0.11126826	0.11106868	0.11108882	0.1111667

5.2 Comparing $(UA)_{Exp}$ and $(UA)_{Th}$

A comparison between the experimental and theoretical thermal conductance was made. Graphing experimental and theoretical thermal conductance versus volume flow rate for each of the variac heater power settings enabled a comparison of the two methods. Error bars were placed on the experimental thermal conductance data points to indicate the uncertainty, d(UA), values previously calculated. Figures 5.3 to 5.6, display these results.

As expected, both experimental and theoretical thermal conductance increased as the volume flow rate was increased for all cases studied. For the lowest power setting on the variac of 30, Figure 5.3, all of the data points' error bars lie within the theoretical plot. Both graphs follow the same trend but the experimental line was off set on the UA axis by an average factor of approximately 0.0191 W/K below the theoretical line.

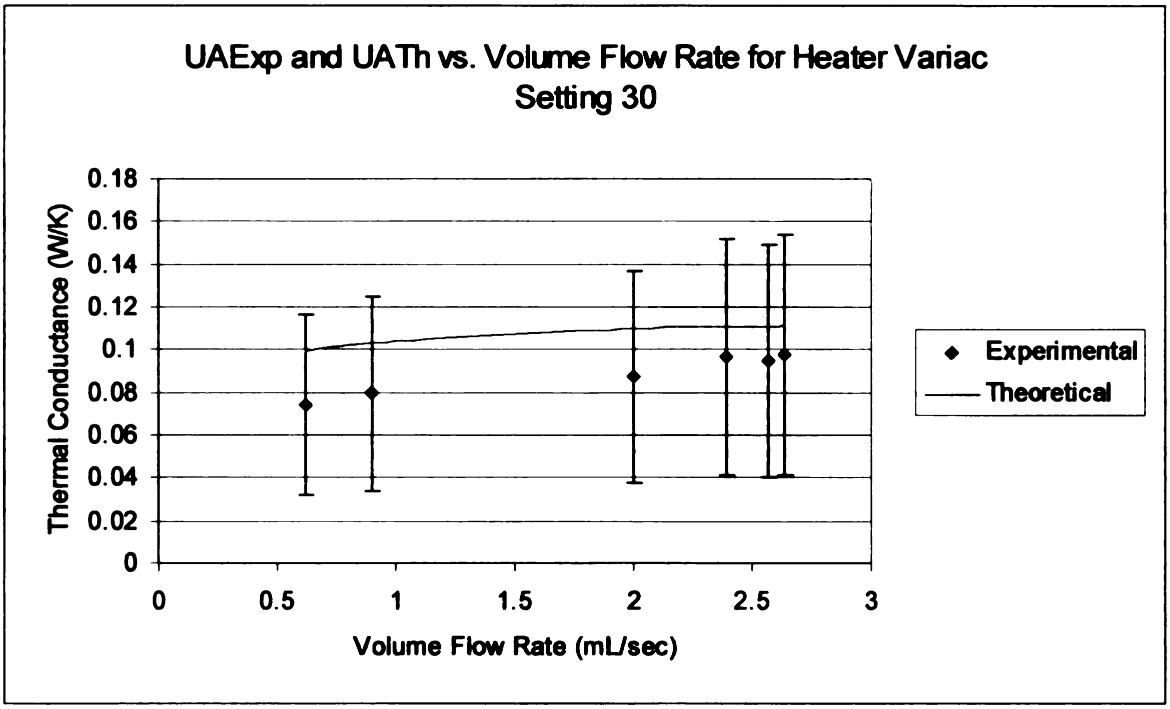

Figure 5.3 $(UA)_{Exp}$ and $(UA)_{Th}$ vs.Volume Flow Rate for Heater Variac Setting 30.

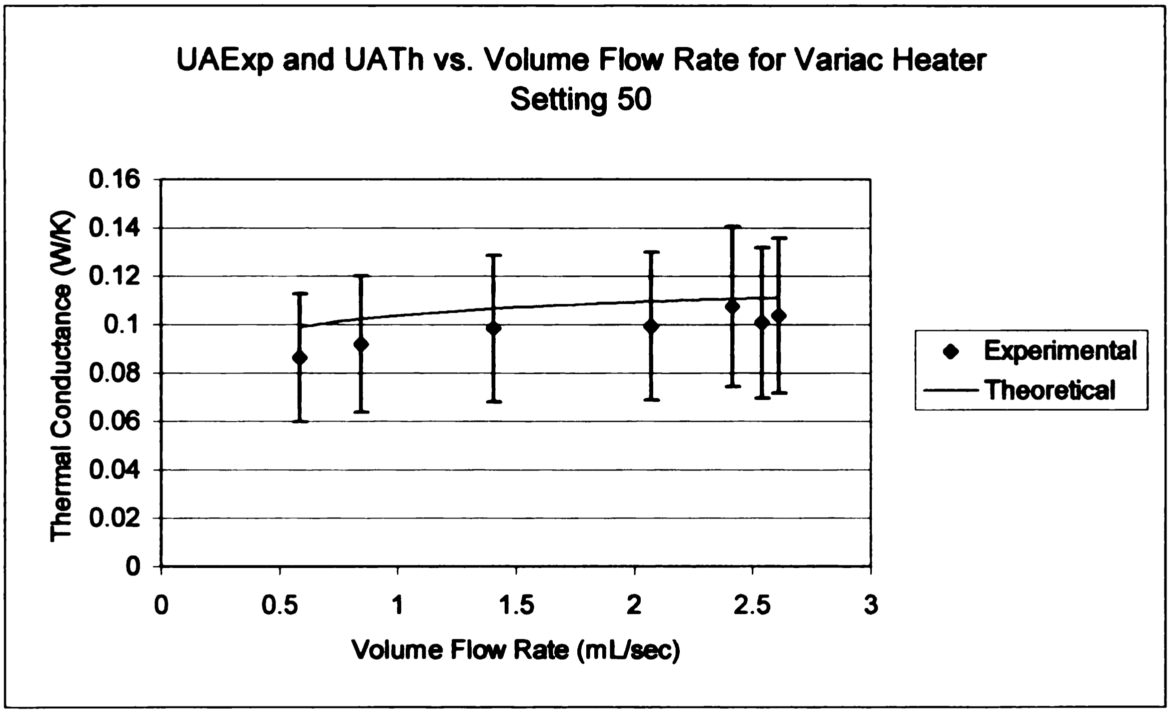

Figure 5.4 $(UA)_{Exp}$ and $(UA)_{Th}$ vs. Volume Flow Rate for Heater Variac Setting 50.

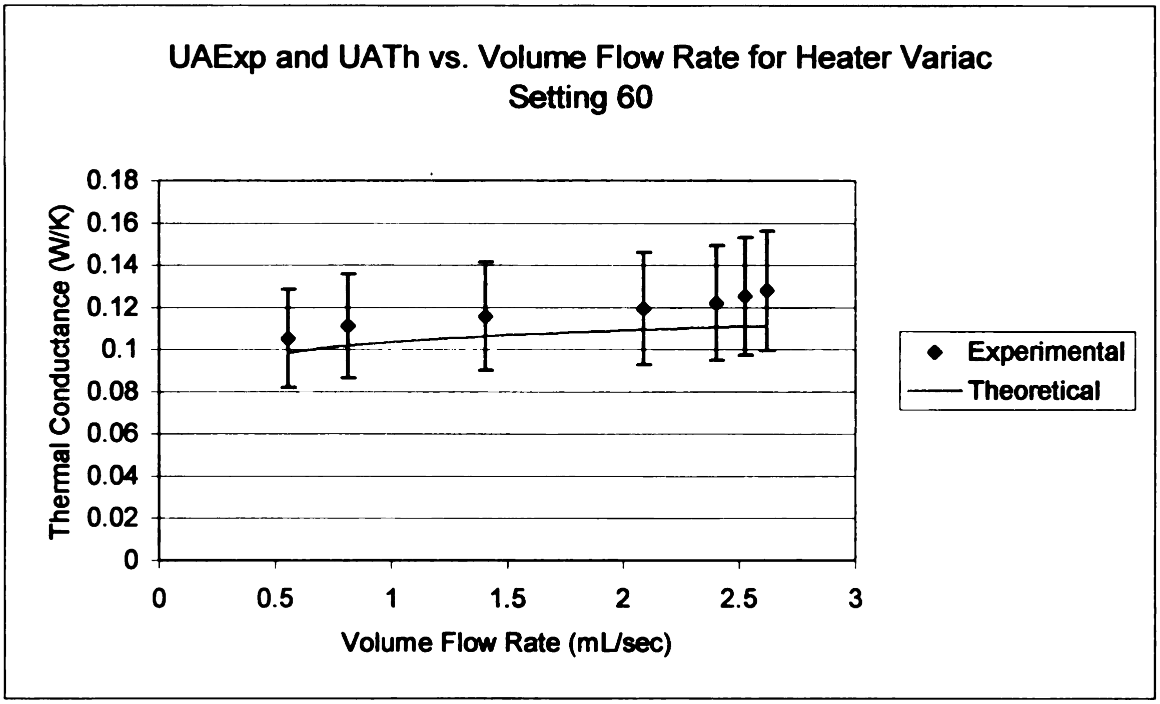

Figure 5.5 $(UA)_{Exp}$ and $(UA)_{Th}$ vs. Volume Flow Rate for Heater Variac Setting 60.

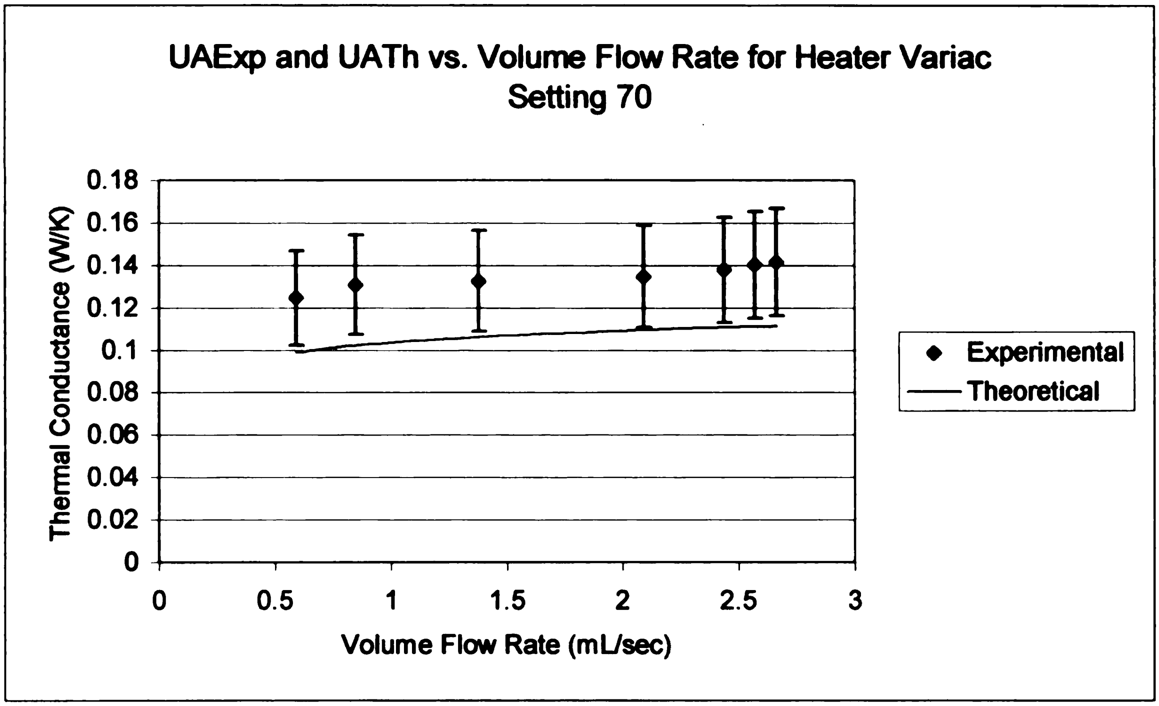

Figure 5.6 $(UA)_{Exp}$ and $(UA)_{Th}$ vs. Volume Flow Rate for Heater Variac Setting 70.

The next power setting on the variac was 50, Figure 5.4, and again all of the data points' error bars lie within the theoretical plot. Both graphs follow the same trend. The average distance that the experimental data points were below the theoretical line was 0.0089 W/K.

The next power setting on the variac was 60, Figure 5.5, and again all of the data points' error bars lie within the theoretical plot. Both graphs follow the same trend but now the experimental data points were above the theoretical line. The average distance that the experimental data points were above the theoretical line was 0.0112 W/K.

The final power setting on the variac was 70, Figure 5.6. This time none of the experimental error bars lie within the theoretical plot but they are in a close proximity. Both graphs follow the same trend. The average distance that the experimental data points were above the theoretical line was 0.0276 W/K. Figures 5.3 to 5.6 proved that the experimental and theoretical thermal conductance were very similar. They followed the same trends and if they are not within the uncertainty they are within a close proximity.

Chapter 6

Conclusion

6.1 Discussion

This work was set out to design, manufacture, and test a device for testing a microscale heat exchanger. In doing so, the performance of the heat exchanger could be viewed by the manufacturers of the device itself. A mathematical model was also analyzed to check the validity of the testing apparatus.

The building of the testing device was successful. It was able to accurately measure the appropriate temperatures, flow rates, voltages, and currents in order to analyze the heat exchanger performance. The key to manufacturing such a device was to mill the edges of the acrylic to obtain a smooth surface. Smooth surfaces bonded better together with the aid of methylene chloride to ensure a watertight seal. Three previous experimental devices were manufactured but failed to be watertight.

The testing of the microscale heat exchanger was also successful. Test runs ran quite smoothly collecting all of the necessary data. The flow rate measurement device that was manufactured allowed for accurate measurements of volume flow rates. With all of the data collected the thermal conductance of the heat exchanger could be calculated.

As intuition would assume, the thermal conductance increased as the volume flow rate was increased. This was because an increase in flow rate resulted in an increase in the convective heat transfer coefficient. As the convective heat transfer coefficient decreased so did R_{Conv}, which was directly proportional to R_{Tot}. Since thermal conductance and R_{Tot} were inversely proportional, UA increased with an increased volume flow rate.

Figure 4.1 showed that for larger heater power settings the microscale heat exchanger would perform better. This increased performance was based on the increase in thermal conductance. Recall Equation 4.2, the increase in power (voltage and current) from one power setting to the next was more than the increase in temperature difference (temperature of heat exchanger minus water temperature). Therefore UA increased with an increase in power supplied to the heat exchanger.

Figures 5.3 to 5.6 displayed the experimental and theoretical thermal conductances versus volume flow rate on the same graph; the heater power varied from graph to graph. The theoretical lines from one graph to the next were almost identical. This was because the theoretical values were not based upon the power supplied to the heat exchanger. They were based purely on the geometry of the heat exchanger, thermo physical properties of water, and the volume flow rate. It was evident that as the power was increased, the experimental values started to rise on the y-axis, an increase in UA. At a power setting of 30 the theoretical line was just above the experimental data points. At a power setting of 50 the theoretical line stayed relatively the same, but the experimental data points moved closer to the theoretical line. At a power setting of 60 the experimental data points rose even higher and were above the theoretical line. The same was evident for a power setting of 70, but the experimental data points increased enough so that the error bars were no longer through the theoretical line.

It should be noted that the conductive contribution to the total thermal resistance, Equation 5.2, was dominant over the convective contribution. The conductive contribution was anywhere from 2.57-4.35 times the convective contribution. Therefore the thermo physical property of thermal conductivity for the microscale heat exchanger was very important.

6.2 Recommendations

The following recommendations are for the testing of the microscale heat exchanger.

- Investigate different lengths of testing channels.
- Test with various temperatures of water, how does it affect UA?
- Experiment with other cooling liquids other than water, which liquid results in the greatest UA?
- With different equipment it would be possible to test at higher volume flow rates. Is it possible to get developed flow, or even turbulent flow? Is there a maximum UA that can be achieved? At what volume flow rate does this occur?
- The testing device manufactured was custom made for one heat exchanger. Is there a way to build a testing device where different sized heat exchangers can easily be changed? Keeping the device watertight would be a major issue.
- Consider heat loss from the top of the heat exchanger or insulate the top.
- Time permitting, the testing of multiple microscale heat exchangers would have been completed.

The following recommendations are for the manufacturing of the microscale heat exchanger.

- Consider hydrodynamic and thermal entry lengths when building microscale heat exchangers as developing laminar flows actually improve the heat transfer. A turbulent flow would increase heat exchanger performance further. Fully developed laminar flow would hinder the performance of the heat exchanger.
- Zirconia has a relatively small thermal conductivity, are there other possible materials to use with a larger thermal conductivity? An increase in thermal conductivity would increase microscale heat exchanger performance because the conductive contribution dominates over the convective contribution to the total thermal resistance.

6.3 Final Remarks

- A successful testing apparatus was manufactured for the microscale heat exchanger.
- The microscale heat exchanger was experimentally analyzed.
- The performance of the microscale heat exchanger was evaluated for various heat supplies and volume flow rates.
- The experiment was compared to a mathematical model.
- The theoretical model confirmed the validity of the experiment.
- Recommendations were made for the testing and manufacturing of the microscale heat exchanger.

BIBLIOGRAPHY

[1] Tien, C. L., and Chen, G., 1994, "Challenges in Microscale Conductive and Radiative Heat Transfer," Journal of Heat Transfer, Vol. 116, pp. 799-807.

[2] Chen, G., 2002, "Ballistic-Diffusive Equations for Transient Heat Conduction From Nano to Macroscales," Journal of Heat Transfer, Vol. 124, pp. 320-328.

[3] Yang, R., Chen, G., and Taur, Y., 2002, "Ballistic-Diffusive Equations for Multidimensional Nanoscale Heat Conduction," Twelfth International Heat Transfer Conference, Grenoble (France).

[4] Tuckermann, D. B., and Pease, R. F., 1981, "High Performance Heat Sinking for VLSI," IEEE Electronic Device Letters, Vol. EDL-2, pp. 126-129.

[5] Tuckermann, D. B., and Pease, R. F., 1982, "Optimized Convective Cooling Using Micromachined Structure," Journal of Electochem. Society, Vol. 129, No. 3, pp. C98.

[6] Wang, B. X., and Peng, X. F., 1994, "Experimental Investigation on Liquid Forced Convection Heat Transfer Through Microchannels," Journal of Heat Transfer, Vol. 37, Suppl. 1, pp. 73-82.

[7] Peng, X. F., Peterson, G. P., and Wang, B. X., "Heat Transfer Characteristics of Water Flowing Through Microchannels," Experimental Heat Transfer, 7 pp. 265-283, Taylor & Francis.

[8] Peng, X. F., and Peterson, G. P., 1996, "Forced Convection Heat Transfer of Single-Phase Binary Mixtures Through Microchannels," Experimental Thermal And Fluid Science 12, pp. 98-104, Elsevier Science Inc.

[9] Gao, P., Le Person, S., and Favre-Marinet, M., 2002, "Hydrodynamics and Heat Transfer in a Two-Dimensional Microchannel," Twelfth International Heat Transfer Conference, Grenoble (France).

[10] Hapke, I., Boye, H, Schmidt, J., and Staate, Y., 2000, "Evaporation in Micro Heat Exchangers," Chem. Eng. Technol. 23 (2000) 6, pp. 496-500.

[11] Kim, S. J., and Kim, D., 1999, "Forced Convection in Microstructures for Electronic Equipment Cooling," Journal of Heat Transfer, Vol. 121, pp. 639-645.

[12] Babin, B. R., Peterson, G. P., and Wu, D., 1990, "Steady-State Modeling and Testing of a Micro Heat Pump," Journal of Heat Transfer, Vol. 112, pp. 595-601.

[13] Jayan, P. G., 2001, "Optimization of Microchannel Heat Sink," Mini Project Report submitted towards partial fulfillment of the requirement for the award Degree of Master of Technology for the Department of Aerospace Engineering at the Indian Institute of Technology in Bombay.

[14] Shin, H. W., 2002, "Fabrication of Functionally Gradient Materials with Internal Channels in Ceramics and Ceramic Composites," A Thesis submitted to Michigan State University in partial fulfillment of the requirements for the Degree of Master of Science, Department of Material Science and Mechanics Engineering.

[15] Incropera, F. P., and DeWitt, D. P., 1990, Fundamentals of Heat and Mass Transfer, 3rd Edition, John Wiley & Sons, New York, pp. 494.

APPENDIX A

LabVIEW program and two sub VIs for obtaining time and voltage data.

Connector Pane

TGPIBpressurebooya.vi

A device connected to a GPIB bus can be written to or be read from using this VI. Select the GPIB address of the device, choose Read or Write or both, type in the characters to be written, and run the VI. If you choose both Read and Write, the VI will write to the device first, then read from the device. Before using this VI you should initialize the GPIB address according to the device's specifications with the "GPIB Initialization" function.

TGPIBpressurebooya.vi
E:\me412\users\dan\TGPIBpressurebooya.vi
Last modified on 10/7/02 at 11:38 AM
Printed on 12/11/02 at 11:47 AM

Front Panel

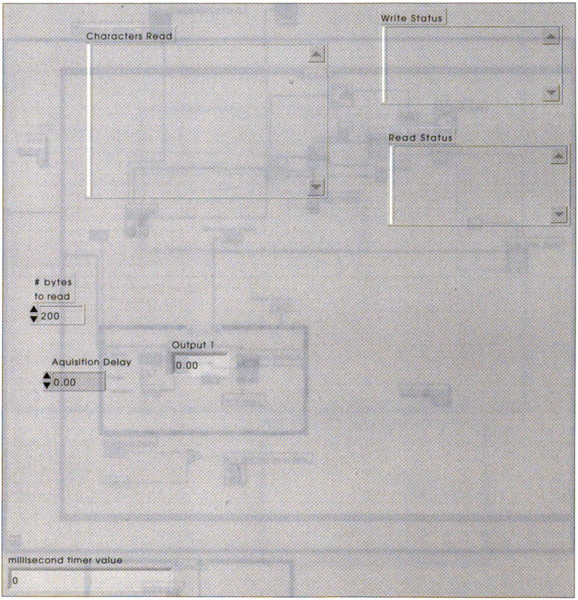

TGPIBpressurebooya.vi
E:\me412\users\dan\TGPIBpressurebooya.vi
Last modified on 10/7/02 at 11:38 AM
Printed on 12/11/02 at 11:47 AM

Block Diagram

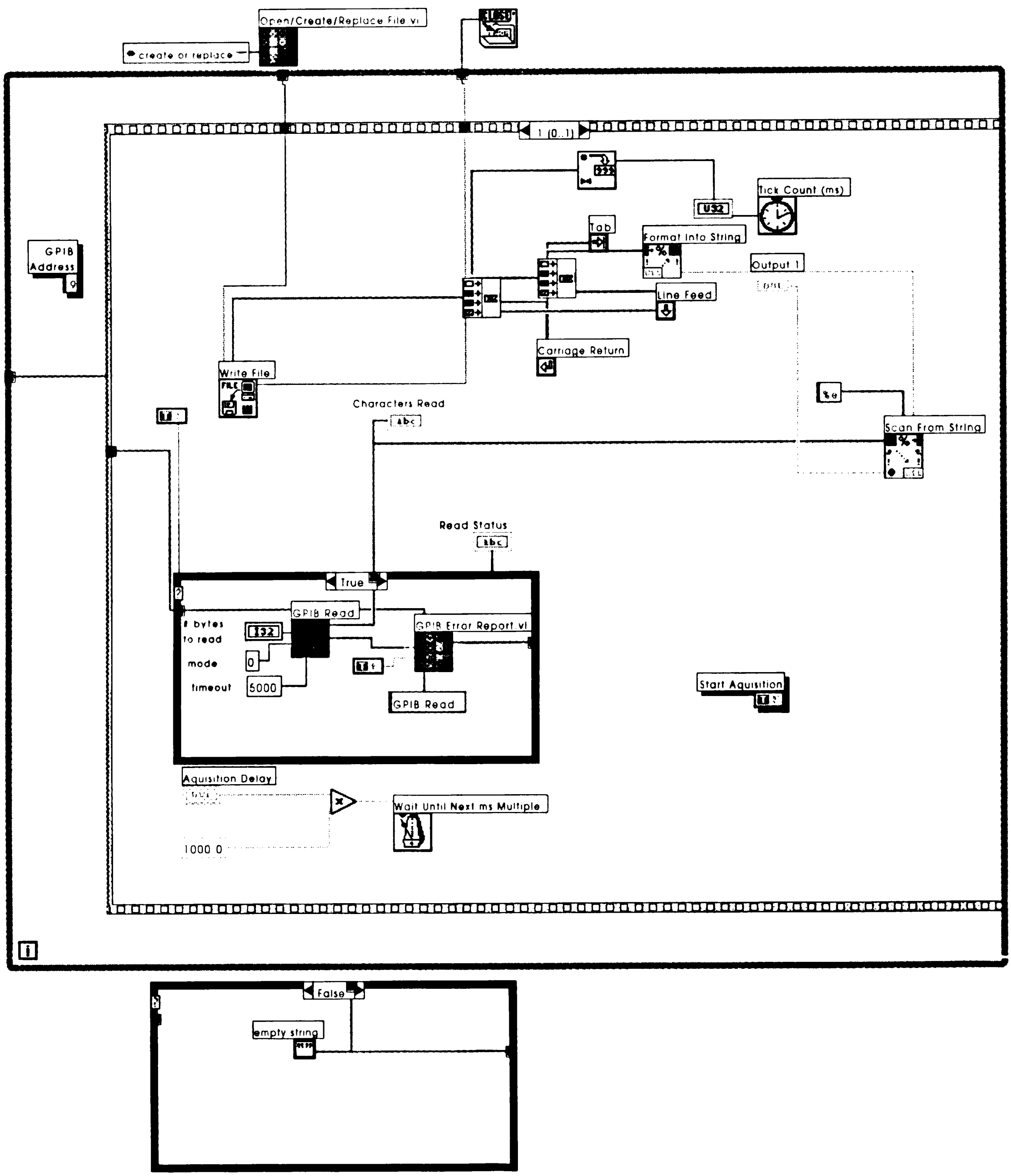

TGPIBpressurebooya.vi
E:\me412\users\dan\TGPIBpressurebooya.vi
Last modified on 10/7/02 at 11:38 AM
Printed on 12/11/02 at 11:47 AM

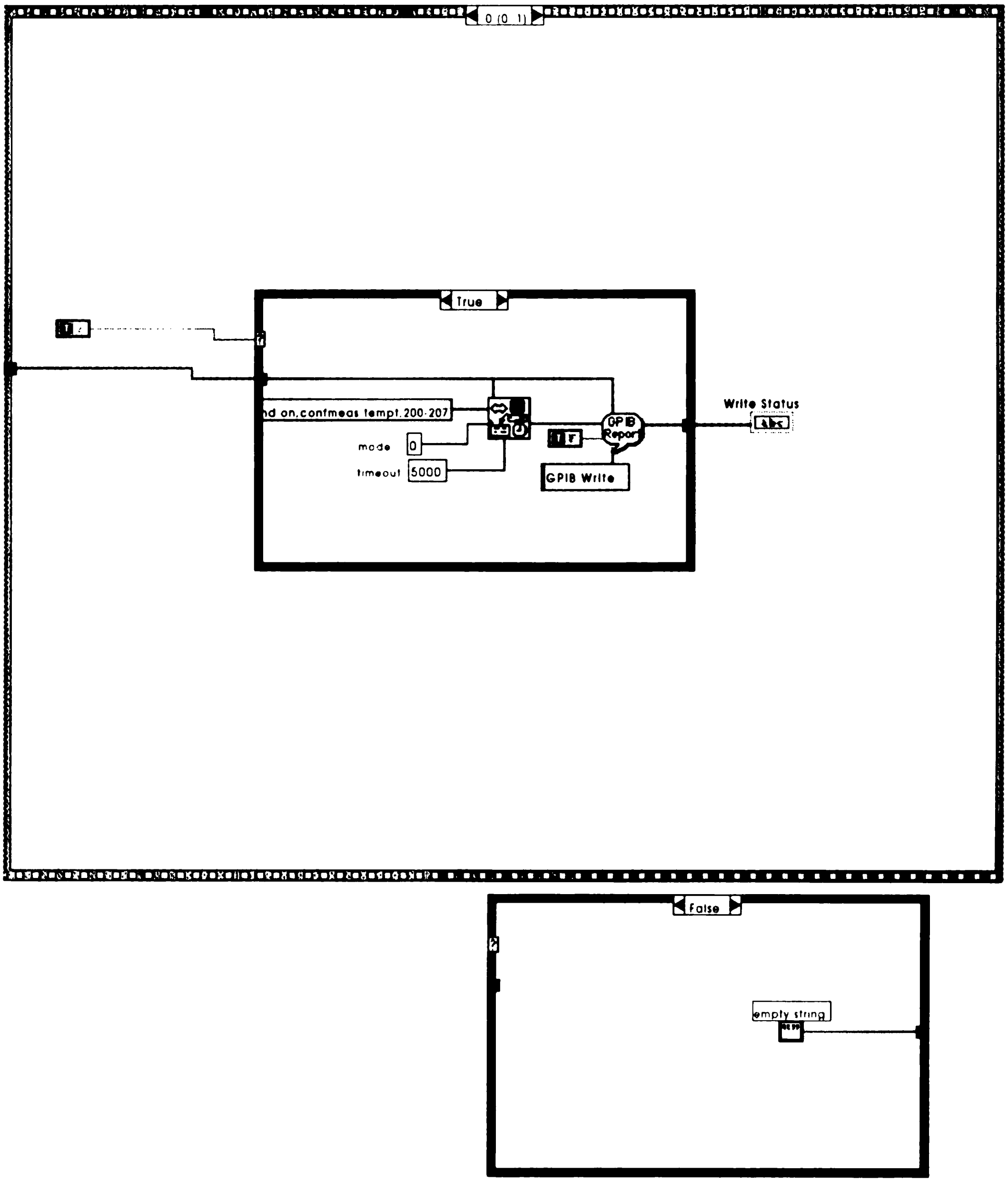

TGPIB4.vi
E:\me412\TGPIB4.vi
Last modified on 2/14/02 at 9:12 AM
Printed on 12/11/02 at 11:48 AM

Connector Pane

TGPIB4.vi

A device connected to a GPIB bus can be written to or be read from using this VI. Select the GPIB address of the device, choose Read or Write or both, type in the characters to be written, and run the VI. If you choose both Read and Write, the VI will write to the device first, then read from the device. Before using this VI you should initialize the GPIB address according to the device's specifications with the "GPIB Initialization" function.

TGPIB4.vi
E:\me412\TGPIB4.vi
Last modified on 2/14/02 at 9:12 AM
Printed on 12/11/02 at 11:48 AM

Front Panel

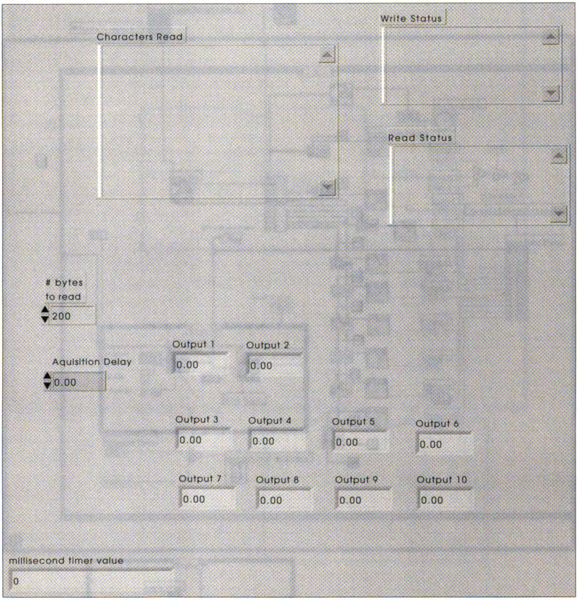

TGPIB4.vi
E:\me412\TGPIB4.vi
Last modified on 2/14/02 at 9:12 AM
Printed on 12/11/02 at 11:48 AM

Block Diagram

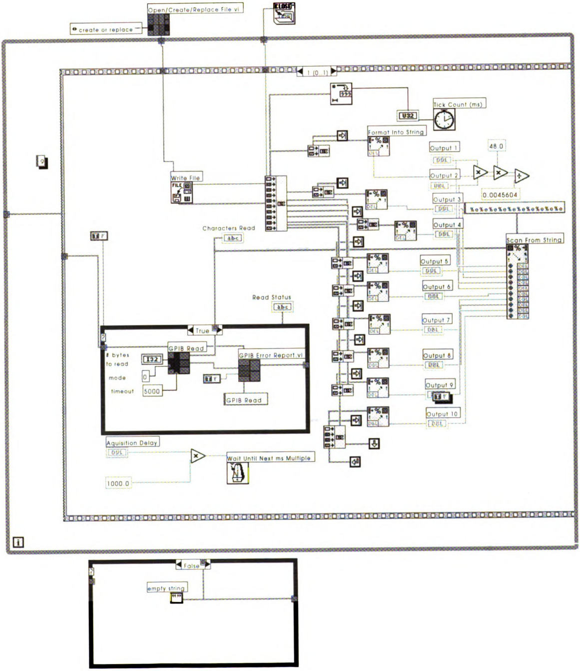

TGPIB4.vi

E:\me412\TGPIB4.vi

Last modified on 2/14/02 at 9:12 AM

Printed on 12/11/02 at 11:48 AM

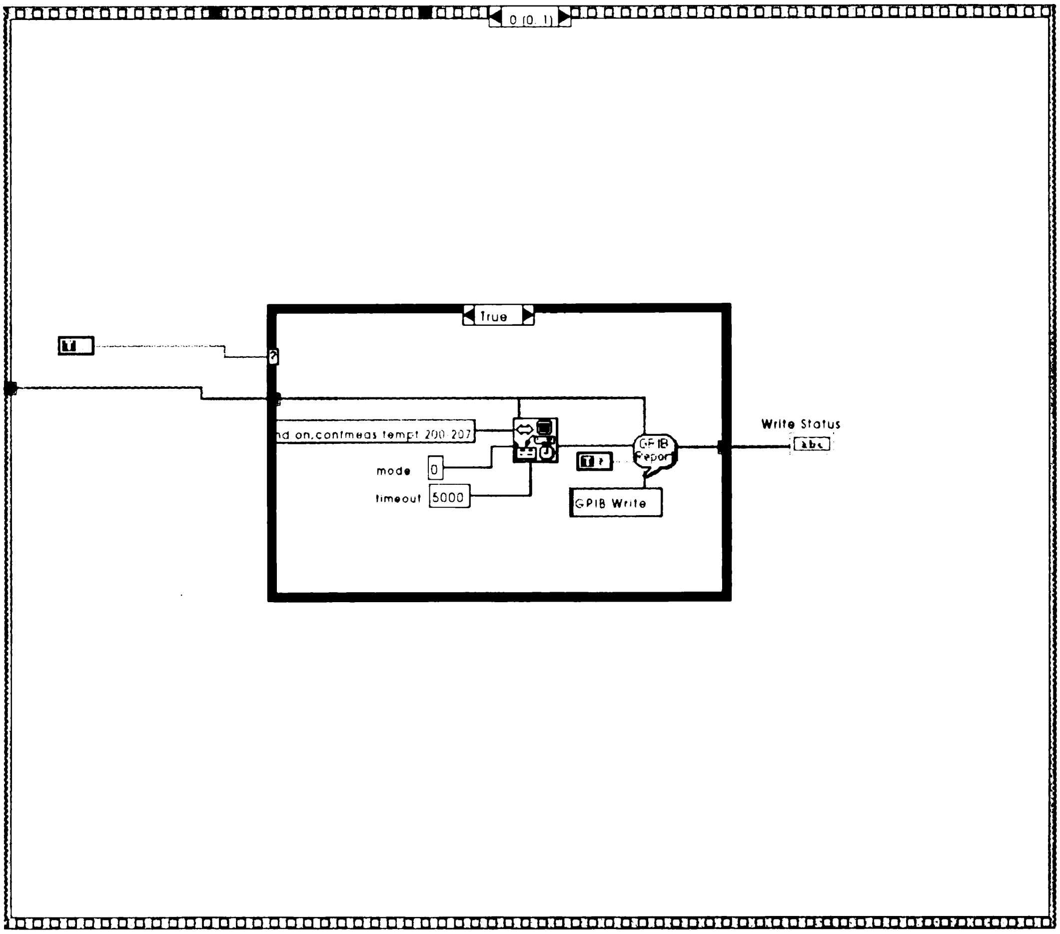

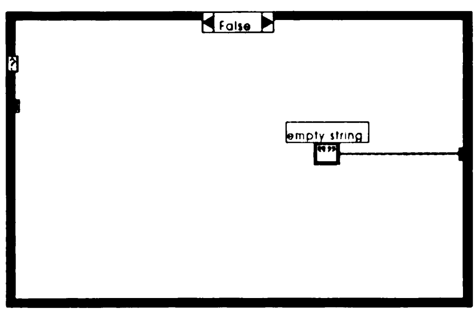

GPIB Error Report.vi
E:\me412\users\dan\GPIB Error Report.vi
Last modified on 10/3/02 at 1:10 PM
Printed on 12/11/02 at 11:48 AM

Connector Pane

GPIB Error Report.vi

Interpret the Status bits returned by a GPIB function and report the status and any error as text. If Dialog is True, the error message will be reported in a dialog box, and the user will have the choice of aborting or continuing.

Front Panel

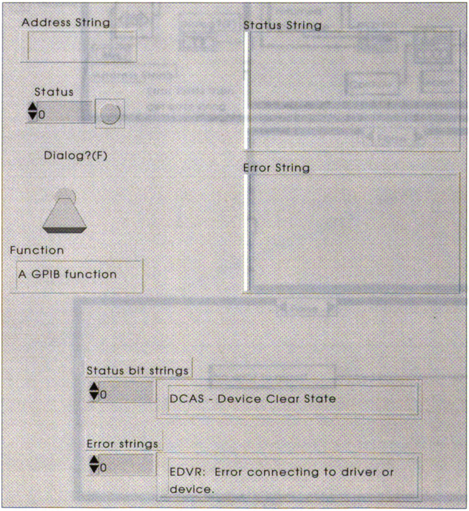

GPIB Error Report.vi
E:\me412\users\dan\GPIB Error Report.vi
Last modified on 10/3/02 at 1:10 PM
Printed on 12/11/02 at 11:48 AM

Block Diagram

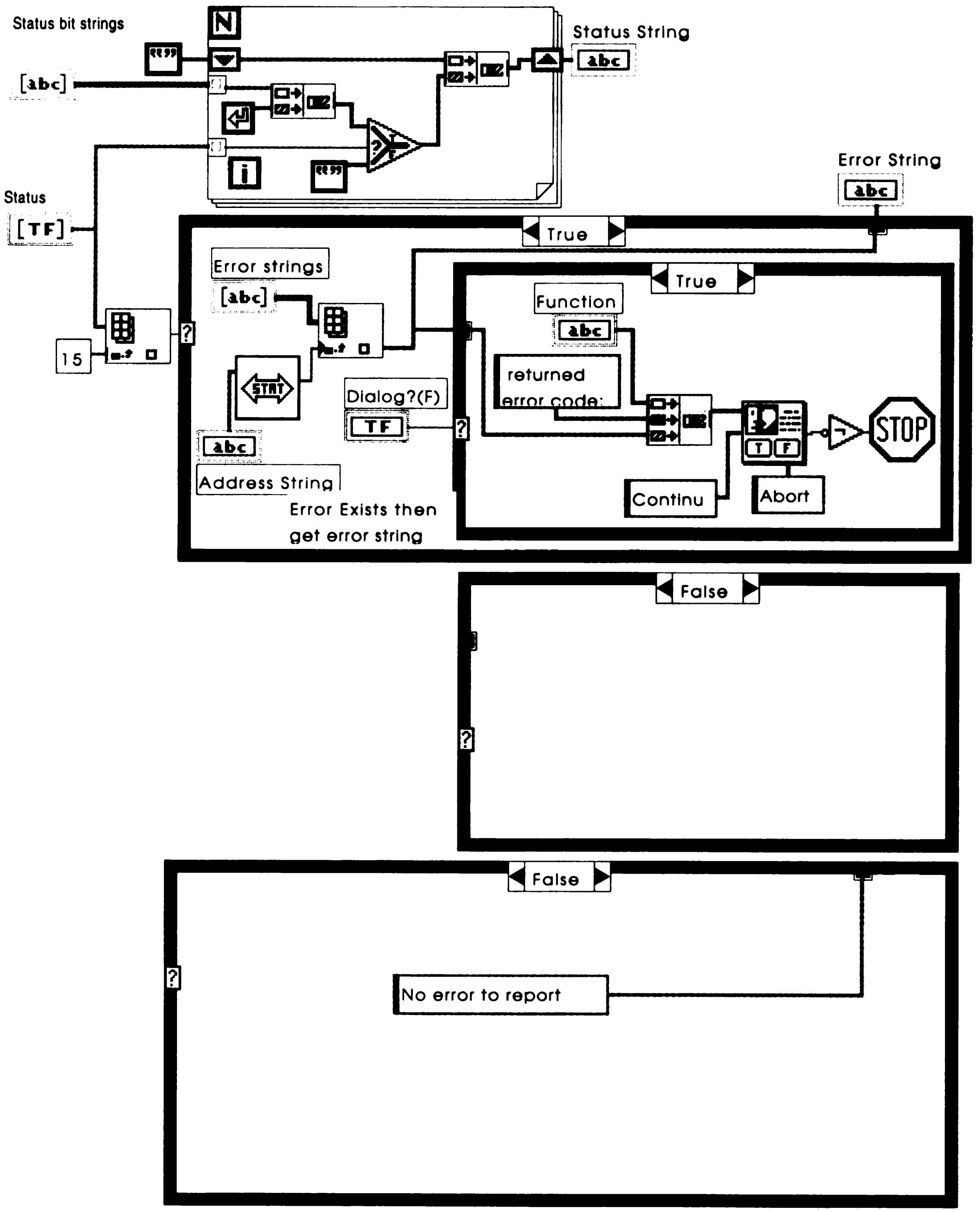

APPENDIX B

A sample of Voltage vs. Time Graphs. Linear fit line was applied to data and slope was used for volume flow rate calculation as described in Section 3.2. There are two numbers in the title of each graph, the first number applies to the heater variac setting and the second number applies to the pump variac setting. An a denotes the second measurement for that particular test run.

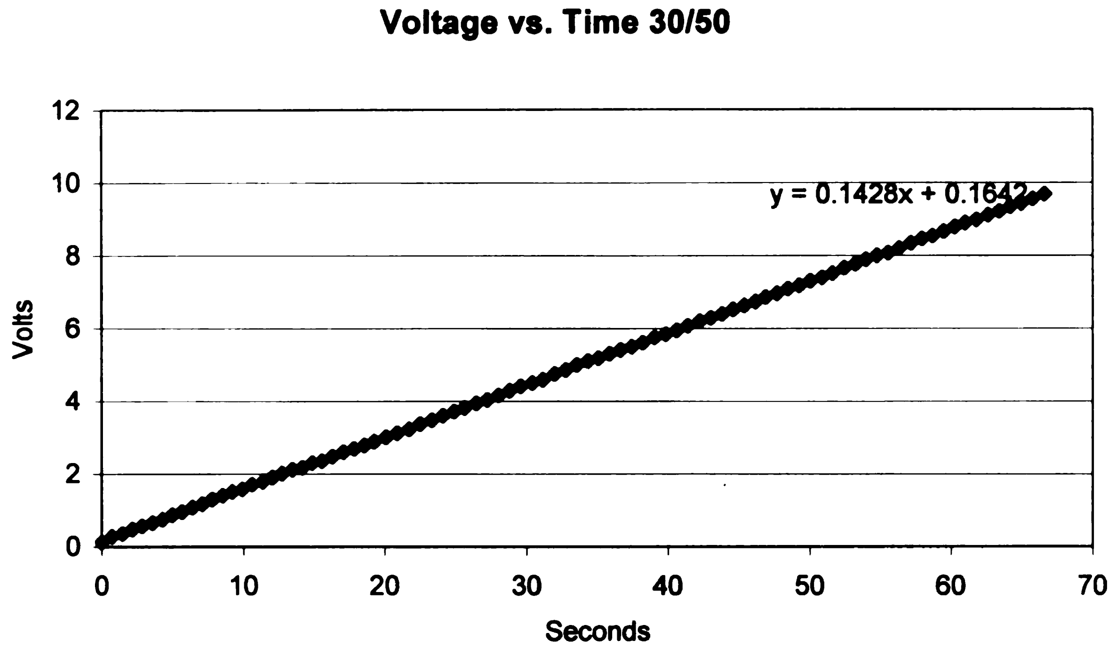

Figure B.1 Voltage vs. Time Graph to Obtain Volume Flow Rate.

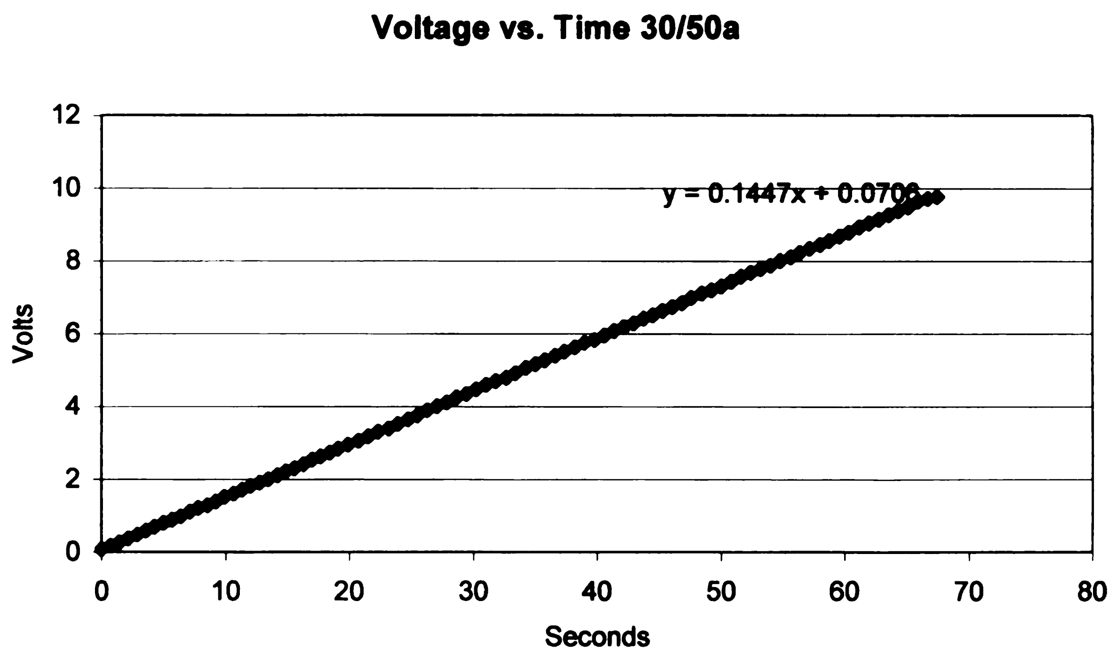

Figure B.2 Voltage vs. Time Graph to Obtain Volume Flow Rate.

APPENDIX C

Excel Spreadsheet containing all data collected in experiment. The spreadsheet also contains all calculations for this thesis, both experimental and theoretical. Note: All rows fit on one page, there were too may columns so there are nine pages.

H Variac	FR Variac	V (Volts)	I (Amps)	Tin (C)	T3 (C)	Tout (C)
30	50	31.8	0.01	22.8	27.4	23.4
30	60	31.8	0.01	23.2	27.5	23.8
30	70	31.8	0.01	23.8	27.7	24.3
30	80	31.8	0.01	24.4	27.9	24.8
30	90	31.8	0.01	24.7	28.3	25.2
30	100	31.8	0.01	25.4	28.9	25.9
50	50	52.6	0.02	21	33.8	22.2
50	60	52.6	0.02	21.2	33.2	22.3
50	65	52.6	0.02	21.3	32.4	22.1
50	70	52.6	0.02	21	32	21.8
50	80	52.6	0.02	21.5	31.7	22.3
50	90	52.6	0.02	20.8	31.6	21.5
50	100	52.6	0.02	20.4	30.9	21.1
60	50	63.3	0.03	20.2	39.1	21.9
60	60	63.3	0.03	20.4	38.2	21.8
60	65	63.3	0.03	19.9	36.9	21.1
60	70	63.3	0.03	20	36.4	21
60	80	63.3	0.03	19.8	35.8	20.7
60	90	63.3	0.03	20	35.6	20.9
60	100	63.3	0.03	20.2	35.5	21.1
70	50	72.9	0.04	17.6	42	19.6
70	60	72.9	0.04	17.8	40.9	19.4
70	65	72.9	0.04	17.9	40.6	19.3
70	70	72.9	0.04	18.3	40.5	19.4
70	80	72.9	0.04	18.6	40.3	19.7
70	90	72.9	0.04	18.9	40.2	19.9
70	100	72.9	0.04	19.2	40.3	20.2

Flow Rate (mL/sec)	Flow Rate (mm^3/sec)	slope (V/sec)	UA	NTU
0.618177695	618.1776954	0.14375	0.073953	0.028729
0.894691266	894.6912663	0.20805	0.0795	0.02134
1.998380348	1998.380348	0.4647	0.087123	0.010471
2.394014073	2394.014073	0.5567	0.096364	0.009668
2.565383681	2565.383681	0.59655	0.094925	0.008888
2.6324694	2632.4694	0.61215	0.097846	0.008929

0.585494909	585.4949094	0.13615	0.08623	0.035362
0.844591996	844.5919957	0.1964	0.091878	0.02612
1.403854669	1403.854669	0.32645	0.098318	0.016816
2.07148658	2071.48658	0.4817	0.099245	0.011503
2.414010778	2414.010778	0.56135	0.107347	0.010677
2.540011519	2540.011519	0.59065	0.10067	0.009516
2.610107494	2610.107494	0.60695	0.103645	0.009533

0.555177325	555.177325	0.1291	0.105208	0.045497
0.814059393	814.059393	0.1893	0.111053	0.032753
1.404929761	1404.929761	0.3267	0.115793	0.019786
2.086537863	2086.537863	0.4852	0.119434	0.013742
2.401324696	2401.324696	0.5584	0.122122	0.012209
2.524745217	2524.745217	0.5871	0.125347	0.011919
2.618708227	2618.708227	0.60895	0.127879	0.011724

0.590225313	590.2253126	0.13725	0.124615	0.050675
0.847387234	847.3872339	0.19705	0.130762	0.037038
1.378912543	1378.912543	0.32065	0.132545	0.023071
2.088903065	2088.903065	0.48575	0.134688	0.015476
2.436372684	2436.372684	0.56655	0.137872	0.013583
2.568608956	2568.608956	0.5973	0.140192	0.013101
2.661926911	2661.926911	0.619	0.141553	0.012765

dU	Re	Qbal	Tavg
0.042081	278.448	0.205891615	23.1
0.045341	406.5148	0.142265485	23.5
0.049845	919.0166	0.076437132	24.05
0.055342	1114.497	0.079761698	24.6
0.054483	1203.695	0.059549335	24.95
0.056227	1254.971	0.058036639	25.65

0.026481	255.4444	0.359508929	21.6
0.028252	369.646	0.271883082	21.75
0.030278	613.7697	0.224909137	21.7
0.03057	899.9974	0.152416354	21.4
0.033128	1059.86	0.130797794	21.9
0.031019	1097.837	0.142055151	21.15
0.031958	1118.856	0.138233574	20.75

0.023315	239.4608	0.483074498	21.05
0.024636	351.4862	0.400049027	21.1
0.025709	599.1616	0.270414749	20.5
0.026535	889.8475	0.218494226	20.5
0.027145	1018.885	0.210940453	20.25
0.027878	1075.63	0.200633557	20.45
0.028454	1120.239	0.193439156	20.65

0.022293	239.0379	0.592901395	18.6
0.023413	343.187	0.51621236	18.6
0.023738	558.4517	0.362548023	18.6
0.024129	852.1782	0.304601672	18.85
0.024711	1002.727	0.261169464	19.15
0.025135	1065.007	0.272504557	19.4
0.025384	1113.631	0.262960905	19.7

Density kg/m^3	Density kg/mm^3	Density kg/mL	mdot kg/sec
996.15	9.9615E-07	0.00099615	0.000615798
996.0833333	9.96083E-07	0.000996083	0.000891187
995.9916667	9.95992E-07	0.000995992	0.00199037
995.9	9.959E-07	0.0009959	0.002384199
995.8416667	9.95842E-07	0.000995842	0.002554716
995.725	9.95725E-07	0.000995725	0.002621216
996.4	9.964E-07	0.0009964	0.000583387
996.375	9.96375E-07	0.000996375	0.00084153
996.3833333	9.96383E-07	0.000996383	0.001398777
996.4333333	9.96433E-07	0.000996433	0.002064098
996.35	9.9635E-07	0.00099635	0.0024052
996.475	9.96475E-07	0.000996475	0.002531058
996.5416667	9.96542E-07	0.000996542	0.002601081
996.4916667	9.96492E-07	0.000996492	0.00055323
996.4833333	9.96483E-07	0.000996483	0.000811197
996.5833333	9.96583E-07	0.000996583	0.00140013
996.5833333	9.96583E-07	0.000996583	0.002079409
996.625	9.96625E-07	0.000996625	0.00239322
996.5916667	9.96592E-07	0.000996592	0.00251614
996.5583333	9.96558E-07	0.000996558	0.002609696
996.9	9.969E-07	0.0009969	0.000588396
996.9	9.969E-07	0.0009969	0.00084476
996.9	9.969E-07	0.0009969	0.001374638
996.8583333	9.96858E-07	0.000996858	0.00208234
996.8083333	9.96808E-07	0.000996808	0.002428597
996.7666667	9.96767E-07	0.000996767	0.002560304
996.7166667	9.96717E-07	0.000996717	0.002653187

Cp J/kgC		Dynamic Viscosity u (Ns/m^2)	
4180.22	for 22-27C	0.000938605	for 20-30C
4180.3		0.000930425	
4180.41		0.000919178	
4180.52		0.00090793	
4180.59		0.000900773	
4180.73		0.000886458	

4179.92	for 17-22C	0.00096928	for 20-30C
4179.95		0.000966213	
4179.94		0.000967235	
4179.88		0.00097337	
4179.98		0.000963145	
4179.83		0.000978483	
4179.75		0.000986663	

4179.81	for 17-22C	0.000980528	for 20-30C
4179.82		0.000979505	
4179.7		0.000991775	
4179.7		0.000991775	
4179.65		0.000996888	
4179.69		0.000992798	
4179.73		0.000988708	

4179.32	for 17-22C	0.0010447	for 10-20C
4179.32		0.0010447	
4179.32		0.0010447	
4179.37		0.001037075	
4179.43		0.001027925	
4179.48		0.0010203	
4179.54		0.00101115	

Dynamic Viscosity u (Ns/mm^2)	Pr	kw (W/mC)	kw (W/mmC)
9.38605E-07	6.4706	0.602856	0.000602856
9.30425E-07	6.401	0.60356	0.00060356
9.19178E-07	6.3053	0.604528	0.000604528
9.0793E-07	6.2096	0.605496	0.000605496
9.00773E-07	6.1487	0.606112	0.000606112
8.86458E-07	6.0464	0.607344	0.000607344

9.6928E-07	6.7316	0.600216	0.000600216
9.66213E-07	6.7055	0.60048	0.00060048
9.67235E-07	6.7142	0.600392	0.000600392
9.7337E-07	6.7664	0.599864	0.000599864
9.63145E-07	6.6794	0.600744	0.000600744
9.78483E-07	6.8099	0.599424	0.000599424
9.86663E-07	6.8795	0.59872	0.00059872

9.80528E-07	6.8273	0.599248	0.000599248
9.79505E-07	6.8186	0.599336	0.000599336
9.91775E-07	6.923	0.59828	0.00059828
9.91775E-07	6.923	0.59828	0.00059828
9.96888E-07	6.9665	0.59784	0.00059784
9.92798E-07	6.9317	0.598192	0.000598192
9.88708E-07	6.8969	0.598544	0.000598544

1.0447E-06	7.3124	0.594936	0.000594936
1.0447E-06	7.3124	0.594936	0.000594936
1.0447E-06	7.3124	0.594936	0.000594936
1.03708E-06	7.2584	0.595376	0.000595376
1.02793E-06	7.1936	0.595904	0.000595904
1.0203E-06	7.1396	0.596344	0.000596344
1.01115E-06	7.0748	0.596872	0.000596872

hw (W/mm^2C)	Aw (mm^2)	Rcond	Rconv	Rtot	UATh
0.014892937	24.5044227	7.303038743	2.740155	10.04319	0.099569918
0.016853848	24.5044227	7.303038743	2.421344	9.724382	0.102834293
0.022044319	24.5044227	7.303038743	1.851223	9.154262	0.109238733
0.023425886	24.5044227	7.303038743	1.742046	9.045084	0.11055729
0.023980414	24.5044227	7.303038743	1.701762	9.004801	0.111051873
0.024229744	24.5044227	7.303038743	1.684251	8.987289	0.111268256
0.014598774	24.5044227	7.303038743	2.795369	10.09841	0.099025513
0.016498387	24.5044227	7.303038743	2.473512	9.776551	0.102285563
0.019542136	24.5044227	7.303038743	2.088255	9.391294	0.106481604
0.022239397	24.5044227	7.303038743	1.834985	9.138024	0.109432852
0.023418294	24.5044227	7.303038743	1.74261	9.045649	0.110550387
0.02379565	24.5044227	7.303038743	1.714976	9.018014	0.110889156
0.023999636	24.5044227	7.303038743	1.700399	9.003438	0.111068685
0.01433194	24.5044227	7.303038743	2.847414	10.15045	0.098517778
0.016283288	24.5044227	7.303038743	2.506187	9.809225	0.101944849
0.019515865	24.5044227	7.303038743	2.091066	9.394105	0.10644974
0.022266145	24.5044227	7.303038743	1.832781	9.135819	0.109459256
0.023325746	24.5044227	7.303038743	1.749524	9.052563	0.110465952
0.02372532	24.5044227	7.303038743	1.720059	9.023098	0.110826679
0.024022687	24.5044227	7.303038743	1.698768	9.001806	0.111088816
0.014549554	24.5044227	7.303038743	2.804825	10.10786	0.098932869
0.01641362	24.5044227	7.303038743	2.486286	9.789325	0.102152089
0.019305868	24.5044227	7.303038743	2.113811	9.41685	0.106192623
0.022188043	24.5044227	7.303038743	1.839232	9.142271	0.109382015
0.023375266	24.5044227	7.303038743	1.745818	9.048857	0.110511198
0.023807267	24.5044227	7.303038743	1.714139	9.017178	0.110899447
0.024112202	24.5044227	7.303038743	1.692461	8.9955	0.111166698

Qpredict	T3	Lh (hydrodynamic entry length mm)
0.428150648	25.1678094	6.961199489
0.411337173	24.883444	10.16287006
0.398721374	24.7497255	22.97541383
0.364839056	25.3214513	27.86242662
0.372023773	25.4862299	30.09236874
0.36162183	26.1715921	31.37427484
1.208111253	25.2304677	6.386111004
1.171169697	24.4080788	9.241149672
1.139353165	23.8121877	15.34424324
1.159988234	22.7927843	22.49993623
1.083393797	23.0831509	26.49648887
1.158791675	22.4310554	27.44592696
1.127347149	21.9945774	27.97139367
1.778245884	25.9534246	5.986520656
1.743256916	25.0241711	8.787156199
1.745775743	23.0403044	14.97903888
1.740402175	22.4961238	22.24618813
1.717745558	22.1595518	25.47213728
1.679024187	22.2603363	26.8907557
1.649668921	22.3913018	28.00598692
2.315029135	24.5929668	5.975946555
2.277991577	23.6533706	8.579674089
2.336237706	22.0140603	13.96129153
2.368120621	21.634751	21.30445546
2.337311847	21.5132851	25.06818123
2.306708488	21.857222	26.62517583
2.290033984	22.0654647	27.84076302

Lt (thermal entry length mm)	Gz^-1	(UAexp-UAth)	Avg Diff
45.04313741	0.005772	0.02561643	0.019135
65.05253125	0.003997	0.023334293	
144.8668768	0.001795	0.022115445	
173.0145243	0.001503	0.014193653	
185.0289477	0.001405	0.0161265	
189.7014154	0.001371	0.013422102	
42.98874484	0.006048	0.012796004	0.008914
61.96652913	0.004196	0.010407834	
103.024318	0.002524	0.008163847	
152.2435685	0.001708	0.010187569	
176.9806478	0.001469	0.003203449	
186.904018	0.001391	0.010219299	
192.4292028	0.001351	0.007423364	
40.87177248	0.006361	0.006689979	0.011154
59.91610326	0.004339	0.009107783	
103.6998862	0.002507	0.009342943	
154.0103605	0.001688	0.009974706	
177.4516444	0.001465	0.011656234	
186.3986513	0.001395	0.014519856	
193.1544912	0.001346	0.016789972	
43.69851159	0.00595	0.025682516	0.02757
62.73800881	0.004144	0.028610243	
102.0905482	0.002547	0.026352832	
154.6362595	0.001681	0.025306207	
180.3304685	0.001442	0.027361142	
190.0931054	0.001368	0.029292861	
196.9678302	0.00132	0.0303867	